DRY FRICTION IN THE FRENKEL-KONTOROVA-TOMLINSON MODEL: DYNAMICAL PROPERTIES

Michael Weiss* and Franz-Josef Elmer

Institut für Physik, Universität Basel, CH-4056 Basel, Switzerland

Abstract

Wearless friction is investigated in a simple mechanical model called Frenkel-Kontorova-Tomlinson model. We have introduced this model in [Phys. Rev. B, **53**, 7539 (1996)] where the static friction has already been considered. Here the model is treated for constant sliding speed. The motion of the internal degrees of freedom is regular for small sliding velocities or weak interaction between the sliding surfaces. The regular motion for large velocities is strongly determined by normal and superharmonic resonance of phonons excited by the so-called "washboard wave". The kinetic friction has maxima near these resonances. For increasing interaction strength the regular motion becomes unstable due to parametric resonance leading to quasistatic and chaotic motion. For sliding velocities beyond first-order parametric resonance bistability occurs between the strongly chaotic motion (fluid sliding state), where friction is large and a regular motion (solid sliding state), where friction is weak. The fluid sliding state is mainly determined by the density of decay channels of m washboard waves into n phonons. This density describes qualitatively the effectiveness of the energy transfer from the uniform sliding motion into the microscopic, irregular motion of the degrees of freedom at the sliding interface. For a narrow interval of the sliding velocities we also found enhanced friction due to coherent motion. In the regime of coherent motion

non-destructive interactions of dark envelope solitons occur.

PACS numbers: 46.30.Pa, 05.70.Ln, 81.40.Pq

I. INTRODUCTION

The sliding of two solid bodies relative to one another is a non-equilibrium process where the kinetic energy of the uniform motion is transferred into energy of irregular microscopic motion, i.e. into heat. This dissipative process leads to friction, called *dry friction*, which differs from viscous friction. Since more than 200 years the phenomenological laws of dry friction (Coulomb's laws) are well-known and are well established in applied physics [1]. They state that the friction force is given by a material parameter (friction coefficient) times the normal force. The coefficient of static friction (i.e., the force necessary to start sliding) is larger or equal to the coefficient of the kinetic friction (i.e., the force necessary for sliding at a constant velocity).

One cannot expect that Coulomb's law can be derived as rigorously as the laws of viscous friction. The reason is that the latter one can be deduced from the well-established theory of near-equilibrium thermodynamics whereas dry friction works mostly far from thermal equilibrium. In fact Coulomb's laws oversimplify a very complex behavior which involves elastomechanical, plastic, and chemical processes operating on different length and time scales (for a general overview of the interdisciplinary aspects of dry friction see Ref. [2]). Experimentally deviations of Coulomb's law are often found [2]. For example, the kinetic friction depends on the sliding velocity. A common pattern is that it first decreases, then goes through a minimum and finally increases [3]. In the case of a thin lubrication layer (thickness: a few monolayers) one often finds the contrary: The kinetic friction first increases, then goes through a maximum and finally decreases [4].

In the last ten years the interest in dry friction (i.e., friction between solids) has been aroused again due to the possibility of reproducible friction experiments on the mesoscopic and nanoscopic scale (nanotribology) [2]. There is some hope that for such less complex systems an understanding is possible by theoretical modeling [4]. From the general point of view of nonequilibrium thermodynamics there is also some hope that it should be possible to develop a simple model which shows all the basic phenomenological features of dry friction. Like the Ising model in the theory of ferromagnetism it is acceptable that such a model is not realistic in every details. What is more important is that it is on the one hand sufficiently

complex to be a testing ground of basic concepts of the statistical mechanics of dry friction. On the other hand it should be simple enough to get analytical results.

The Frenkel-Kontorova-Tomlinson (FKT) model goes back to an old idea of Tomlinson which explains Coulomb's laws on the atomic level [6,7]. His attempt concerns the most puzzling feature of dry friction, namely, that the friction force remains finite in the limit of quasistatic sliding (i.e., sliding velocity going to zero). It is clear that this behavior cannot be treated, like viscous friction, as the linear response of a system near thermal equilibrium. Tomlinson's idea was that friction is caused by mutual "plucking" of surface atoms. Each plucked surface atom vibrates. Plucking is possible only if the sliding brings surface atoms into metastable states from which they suddenly jump into more stable ones. The energy difference is turned into kinetic energy which is totally dissipated due to the emission of some type of bulk or surface waves (e.g., sound waves) by the plucked atom. This is the basic dissipation channel. Tomlinson's mechanism works even in the limit of quasistatic sliding provided that the barrier between the metastable and the stable states is sufficiently high and the temperature sufficiently low.

This simple picture assumes (i) that the relaxation time of a plucked atom is much smaller than the averaged time between two jumps of the same atom and (ii) that a vibrating atom does not excite vibrations of other surface atoms. These assumptions lead to a kinetic friction that does not depend on the sliding velocity [6,8].

The first assumption does not hold if either the vibration after the jump is not totally dissipated until the next plucking event of the same atom (weak dissipation) or the jump itself occurs on a time scale larger than the averaged time between two plucking events of a single atom (strong dissipation). One can imagine that in the case of atomically flat surfaces such plucking events occur in a regular fashion with a frequency (so-called *washboard frequency* [9]) which is determined by the sliding velocity multiplied by the principal wave number of the surface structure. In the case of weak damping we can therefore expect *resonances* which should lead to a velocity-dependent kinetic friction with resonance peaks. The situation can be modeled by the independent oscillator or Tomlinson model [7,10]. It is a damped harmonic oscillator (eigenfrequency ω_0) interacting with a sliding surface (velocity v) which is described by a spatially periodic potential with wave number k. Two types of resonances

are possible in the Tomlinson model [11]: *Normal resonance* where the oscillator is plucked after n oscillations (resonance condition: $\omega \equiv vk = \omega_0/n$), and *parametric resonance* which is an instability where oscillations are excited due to the modulation of the effective frequency of the oscillator during sliding (resonance condition: $\omega = 2\omega_0/n$, where n is an integer) [12]. In the case of weak interaction these resonances can be calculated analytically, whereas in the case of strong interaction the motion of the oscillator becomes chaotic and pronounced hysteresis occurs [10,11]. The kinetic friction becomes a wild, multi-valued function of the sliding velocity. This is even the case after averaging over an ensemble of *identical* oscillators [13].

The easiest way of taking into account the coupling between surface atoms is to introduce a linear nearest-neighbor interaction of the oscillators. This leads to the Frenkel-Kontorova-Tomlinson model which we have already introduced in Ref. [5]. The FKT model assumes two rigid sliding bodies where the layer of surface atoms of one body is modeled by a mechanical particle-spring model (see Fig. 1). There are two kind of springs, a nearest-neighbor spring and a spring which couples each particle to the body. The interaction between the two bodies is described by a spatially periodic potential. The dissipative coupling of the layer with the environment is modeled by damping terms which are proportional to the relative velocities. The static properties (ground state, meta-stable states, static friction) of the one-dimensional FKT model have already been discussed in Ref. [5]. In this paper we investigate dynamical properties such as the kinetic friction of the one-dimensional FKT model. A brief summary of Ref. [5] and of this paper is given in Ref. [14].

The FKT model is far from being realistic in certain aspects. Its main disadvantages are the following. The assumption of harmonic particle interaction does not hold in the case of strong distortions. The elasticity of the bulk is missing which leads to an artificial gap in the phonon dispersion relation (see Sec. IV A).

The FKT model shares many similarities with the Burridge-Knopoff (BK) model [15], which was proposed as a model of an earthquake fault. There also a linear, harmonic chain of blocks attached via springs at a rigid plate is assumed. But the interaction with the other surface is modeled by phenomenological force describing a dry friction law. Mostly velocity-weakening laws are used. That is, the friction force decreases with the sliding velocity.

The dynamical properties of the BK model have been studied extensively in the literature [16–24].

The paper is organized as follows. In Sec. II the FKT model and the kinetic friction F_K are defined. The behavior for small sliding velocities is treated in Sec. III. Here mostly stick-slip motion of individual particles occurs. At higher velocities excitations of phonons become important. The consequence of several kinds of resonances is discussed in Sec. IV. In the last section we compare our results with other models, especially with the BK model.

II. DEFINITIONS

The Frenkel-Kontorova-Tomlinson (FKT) model has already be introduced in Ref. [5]. Thus the key features are described only briefly. Here we will concentrate more on the dynamical properties of the model which have not been investigated in Ref. [5]. Also a definition of kinetic friction F_K is given.

A. The FKT model

A linear chain of N particles coupled harmonically forms the backbone of the FKT model (see Fig. 1). The particles can move only parallel to the sliding direction. Thus the model is completely one-dimensional. All particles have the same mass which defines the mass unit. Also the nearest-neighbor interaction is assumed to be uniform which defines the force unit. The chain is the interface between two rigid sliding bodies which are modeled in two very different ways. The interaction with the lower body is described by a spatially periodic potential. Its periodicity defines the unit of the length scale. The interaction with the upper body is assumed to be harmonic. That is, each particle is coupled via a spring to the upper body. All springs are identical and they are attached with equal spacing at the upper body. The boundary conditions are assumed to be periodic.

In this paper the motion of the chain is investigated for the case of sliding the upper body against the lower one at constant velocity v. This externally constrained sliding leads to vibrations within the chain. These vibrations excite waves into the bulk of the sliding bodies which carries energy away from the sliding interface. In the FKT model the degrees

of freedom which are responsible for these waves are not explicitly present. We include their effect by introducing two phenomenological damping forces which are proportional to the particle velocity measured relative to the lower and the upper body, respectively. In this paper we investigate the FKT model in the limit of zero temperature where fluctuation forces disappear. Below we will see that the kinetic friction is directly given by the rate of energy which is transferred into these basic dissipation channels.

The equation of motion of the FKT model reads

$$\ddot{\xi}_j + \gamma_L(v + \dot{\xi}_j) + \gamma_U\dot{\xi}_j = \xi_{j+1} + \xi_{j-1} - (2 + \kappa)\xi_j +$$
$$+b\sin 2\pi(vt + cj + \xi_j), \tag{1}$$

where ξ_j is the position of particle j relative to its equilibrium value given by the upper body, c is ratio of the lattice constant of the upper body to that of the lower body, b and κ are the strengths of interaction with the lower and upper body, respectively, and γ_L and γ_U are the damping constants of the particle motion relative to the lower and upper body, respectively. The boundary condition is

$$\xi_{j+N} = \xi_j, \tag{2}$$

which requires

$$c = \frac{M}{N}, \quad \text{with } M \text{ integer.} \tag{3}$$

The transformation

$$t \to t + \gamma_L/\kappa, \quad \xi_j \to \xi_j - \gamma_L v/\kappa \tag{4}$$

turns (1) into

$$\ddot{\xi}_j + \gamma\dot{\xi}_j = \xi_{j+1} + \xi_{j-1} - (2 + \kappa)\xi_j +$$
$$+b\sin 2\pi(vt + cj + \xi_j), \tag{5}$$

with

$$\gamma = \gamma_L + \gamma_U. \tag{6}$$

In addition to the symmetries of the FKT model already mentioned in Ref. [5], eq. (1) is invariant under translation in time by an integer multiple of the inverse sliding velocity. Below we will see that all solutions which do not break this symmetry are defined by a single one-parameter function, the dynamical hull function, which is similar to the static hull function [5].

For the results presented in the following sections, the equation of motion (5) is often integrated numerically. We have done this by using a second-order Runge-Kutta scheme which in the non-damping case is identical with the Verlet algorithm [25]. For the time step we have chosen 0.01. This is sufficient because all simulations are done for $\kappa = 1$ and $v < 1.5$. The corresponding fastest time scale is $2\pi/\sqrt{5}$.

B. The kinetic friction

The kinetic friction F_K is the temporal average of the force necessary to keep the body sliding at a constant velocity v. It is given by the sum of the forces between the particles and the upper body [5],

$$F_K = -\lim_{T\to\infty} \frac{\kappa}{T} \int_0^T \sum_{j=1}^N \xi_j(t)\, dt. \tag{7}$$

There is a second equivalent definition which clearly shows the dissipative nature of the kinetic friction. The idea is that after the decay of transients the energy flows through the system at a constant rate. That is, the energy which is put into the system per unit time by sliding is on average totally dissipated. Thus the total energy (i.e., the kinetic and the potential energy) of the chain is on average constant. With the further assumption that the motion of the ξ's is bounded we get

$$F_K = \gamma_L vN + \lim_{T\to\infty} \frac{\gamma}{vT} \int_0^T \sum_{j=1}^N \dot{\xi}_j^2(t)\, dt. \tag{8}$$

From the last definition we clearly see that the kinetic friction is proportional to the *rate* of energy transfer from the motion of the interface particles into some types of bulk waves. This is a general principle: The kinetic friction is determined by the various rates of energy transfer starting from the uniform macroscopic motion of the sliding bodies and ending in some dissipation channels. For the FKT model we are mainly interested in the efficiency of

the transfer from the macroscopic sliding into microscopic motion of the interface particles. In section IV we will see that this efficiency is rather high if phonons are excited resonantly. That is, the kinetic friction as a function of the sliding velocity shows resonance peaks.

In the following sections we always discuss the kinetic friction without the first term of definition (8). That is, in any plot of F_K versus v one should add $\gamma_L v N$. We will see that for very large velocities this term dominates the second one.

III. THE LOW-VELOCITY REGIME

In this section we investigate the FKT model for very small sliding velocities. In fact we are treating the quasistatic limit $v \to 0$. In Ref. [5] we have already discussed the disappearance of the kinetic friction in this limit if b is less than some critical value b_c^K. Here we investigate F_K as a function of v for b below and above this threshold.

A. $b < b_c^K$

In Ref. [5] we have shown that for $b < b_c^K$ the stationary values of the ξ's follow the quasistatic sliding adiabatically. Furthermore, there is only one stationary state which can be described by the static hull function g_S [defined by Eq. (10) in Ref. [5] which is identical with (37) for $v = 0$]. Therefore, the solution of the equation of motion (5) in the quasistatic limit reads

$$\xi_j(t) = g_S(vt + cj) \quad \text{with} \quad g_S(x + 1) = g_S. \tag{9}$$

Using (8) we immediately see that the kinetic friction behaves viciousely, i.e.,

$$F_K = \gamma_{\text{eff}} v N, \tag{10}$$

with an effective damping constant

$$\gamma_{\text{eff}} = \gamma_L + \gamma \int_0^1 \left(\frac{dg_S}{dx} \right)^2 dx. \tag{11}$$

In the Tomlinson limit (i.e., $\kappa, b \to \infty$) and for $c = 1$ an analytic expression can be obtained (see appendix A). In the limit $b \to b_c^K$ the effective damping constant diverges like

$$\gamma_{\text{eff}} \sim (b_c^K - b)^{-1/2}. \tag{12}$$

B. $b > b_c^K$

For $b > b_c^K$ additional metastable states appear [26]. Due to quasistatic sliding these states eventually annihilate with an unstable counterpart in a saddle-node bifurcation [5]. At those points the chain has to find a new metastable configuration. That is, the particles of the chain no longer move adiabatically. They start to move with finite velocities, and after a transient they reach a new metastable state. The dissipated energy is the difference in potential energy before and after the reconfiguration event. This is the generalization of Tomlinson's friction mechanism. The kinetic friction in the quasistatic limit is therefore the averaged energy drop per jump $\langle \Delta V \rangle$ divided by the averaged distance $\langle \Delta x_B \rangle$ between the relative positions of the sliding bodies between two subsequent reconfiguration events:

$$F_K(v \to 0) = \frac{\langle \Delta V \rangle}{\langle \Delta x_B \rangle}. \tag{13}$$

In the overdamped limit, i.e., $\gamma \to \infty$, the system selects via steepest descent the nearest possible metastable state on the energy surface. Starting with an arbitrary metastable state the system will reach after several jumps a state which can be obtained by adiabatic deformation from the ground state of the undriven FKT model [27]. Then this state always reappears after each jump. The reason for this selection rule is closely related to the fact that the ground state has the highest depinning force of all metastable states [5]. The sequence of reconfiguration events becomes therefore regular. We assume that c is the ratio of two coprime integers P and Q (i.e., $c = P/Q$) where Q is a divisor of N. In each reconfiguration event N/Q equally spaced particles jump into the neighboring potential wells. Each jumping particle together with the neighboring particles dissipates ΔV_0. Thus the totally dissipated energy is $\Delta V_0 N/Q$. The distance between two events is $1/Q$. Thus

$$F_K(v \to 0) = \Delta V_0 N. \tag{14}$$

Near the onset of friction F_K scales like

$$\frac{F_K(v \to 0)}{N} \sim (b - b_c^K)^2. \tag{15}$$

The leading orders of this expansion are calculated in Appendix A for $c = 1$ and for the Tomlinson limit. For $b \gg \kappa \gg 1$ we get (see appendix A)

$$\frac{F_K(v \to 0)}{N} = b\left(1 - \frac{\kappa}{2b} + \frac{\sqrt{2}}{3\pi}\left(\frac{\kappa}{b}\right)^{\frac{3}{2}} + \cdots\right). \tag{16}$$

In the limit $\kappa/b \to 0$ the kinetic friction is approaching the static friction $F_S = F_S^{max} \equiv bN$.

Figure 2 shows for several values of c the static friction F_S and the kinetic friction $F_K(v \to 0)$ which are obtained numerically by solving the delay equation of the hull function g_S. First of all, we notice the excellent agreement between analytical and numerical results for $c = 1$. Furthermore, we observe that the kinetic friction is approaching the static friction from below not only for $b \to \infty$ but also for $Q \to \infty$ (i.e., for decreasing commensurability of c). In fact the difference scales like $1/Q$ for $Q \gg 1$. This can be understood by the following argument. The jumps of the N/Q particles represent a kind of microslip leading to typical stick-slip motion with a sawtooth curve of the lateral force $F = -\kappa \sum_j \xi_j$ as a function of the relative position between the sliding bodies. The maximum of this curve defines F_S whereas the kinetic friction is the average in accordance with definition (7). Thus $F_S - F_K(v \to 0)$ is given by half the height of the jumps which is proportional to $1/Q$ because in each jump N/Q particles are jumping over a distance which is independent of Q for $Q \gg 1$. The jump is roughly proportional to the largest gap in the hull function g_S (see Figs. 2 in Ref. [5]).

If we take inertia into account, i.e., γ finite, the system does not necessarily select the nearest possible minima of the energy landscape. That is, the particle may jump over several potential wells before being captured. This has two consequences: (i) It lowers the kinetic friction which can become zero in the extreme case of $\gamma \to 0$. (ii) It makes the motion irregular. That is, the states between the reconfiguration events are no longer equivalent to the ground state, and ΔV and Δx_B are fluctuating properties.

This irregular behavior is similar to the irregular motion in the BK model [17]. For example, as in the BK model the FKT model shows a power law distribution of ΔV up to a certain cutoff value [28]. This cutoff monotonically decreases with increasing κ. For $\kappa \gtrsim 1$ the power law disappears and the distribution is exponential [28,24]. The power law behavior has also fed the speculation that dry friction may be a self-organized critical process. This subject is not addressed here. The interested reader is referred to Ref. [28] where the FKT model is discussed in this context.

The dynamical behavior of the chain does not change qualitatively if the sliding velocity is

finite but still small. There is again a regular sequence of reconfiguration events where N/Q equally spaced particles jump. It is expected that $F_K(v)$ increases with v because the critical slowing down of the system near a saddle-node bifurcation delays the reconfiguration event. Thus the energy drop ΔV is larger than in the quasistatic limit because at the beginning of the reconfiguration event the strings connecting the particles with the upper body are stretched more. From simulations we find that $dF_K/dv|_{v\to 0}$ is indeed positive (see Figs. 3 and 6). We also see that after reaching a maximum F_K decreases. This can be understood in the following way. In the simulations shown in Figs. 3 and 6 the motion is not overdamped. Therefore the particles oscillate after jumping. If the sliding is sufficiently fast they are still oscillating at the next jumping event. Thus they explore the phase space and may therefore overcome the barrier before it disappears in the saddle-node bifurcation mentioned above. For increasing sliding velocity the delay caused by critical slowing down is more and more compensated by this mechanism. It leads to a local maximum of $F_K(v)$ at a velocity which scales like γ. This is roughly confirmed by the friction curves in Fig. 3.

IV. THE HIGH VELOCITY REGIME

In the previous section we have investigated the FKT model in a regime where Tomlinson's basic dissipation mechanism works, namely, that the energy put into the system is released and subsequently dissipated in recognizable reconfiguration events. For increasing sliding velocity the average time between successive reconfiguration events will eventually become smaller than the average time scale on which such events take place. Reconfiguration events overlap and are no longer recognizable. Thus we have entered a new regime where the particles are always in motion. In this regime the friction may be strongly enhanced due to *resonances of waves*, i.e., phonons.

In this section the consequences of these resonances are investigated on various levels. First we treat the linearized equation of motion. In a second step we calculate numerically all regular solutions which do not break the discrete temporal translation symmetry of the equation of motion. Then irregular solutions are investigated. At the end of this section we report on solitary behavior.

A. The basic resonances

The external potential describing the hard surface of the lower body makes the equation of motion (5) nonlinear. Therefore it is very hard to find analytical solutions. For a weak potential, i.e., $b \ll 1$, and sufficiently strong dissipation one can expect that the oscillations of the particles are small. Thus we can linearize the equation of motion,

$$
\ddot{\xi}_j + \gamma \dot{\xi}_j = \xi_{j+1} - (2+\kappa)\xi_j + \xi_{j-1}
$$
$$
+ b \sin 2\pi(vt + cj)
$$
$$
+ 2\pi b \cos 2\pi(vt + cj) \cdot \xi_j. \tag{17}
$$

Both terms on the right-hand side which are proportional to b can be considered as driving terms. These driving terms are periodic in t and j with frequency $2\pi v$ and wave number $2\pi c$. We call this driving wave the "washboard wave". It leads to different types of resonances. The first driving term is responsible for the *main resonance*. The last term leads to *parametric resonance*. Both terms are responsible for *superharmonic resonance*.

The washboard wave can resonantely excite phonons (i.e., sound waves) which are solutions of (17) for $\gamma = b = 0$. They have the form

$$
e^{i[k_m j \pm \omega(k_m)t]},
$$

with the dispersion relation

$$
\omega(k) = \sqrt{\kappa + 4\sin^2 \frac{k}{2}}. \tag{18}
$$

Because of periodic boundaries, k has to be discrete

$$
k = \frac{2\pi}{N}m, \ m = 0, \ldots, N - 1. \tag{19}
$$

1. The main resonance

We drop the last term of (17). Such linearized equations have already been studied in many other models [29–31]. They can be easily solved by the Ansatz

$$
\xi_j = A \cos[2\pi(vt + cj) + \phi] \tag{20}
$$

which leads to a typical resonance line

$$A = \frac{b}{\sqrt{[\omega^2(2\pi c) - (2\pi v)^2]^2 + (2\pi v\gamma)^2}}. \tag{21}$$

Note that (20) is the solution in the limit $t \to \infty$ where all other solutions have died out because of $\gamma > 0$.

In order to calculate from this solution the kinetic friction one has to be aware that for the linearized equation of motion (17) the two definitions (7) and (8) are no longer equivalent. The first definition (20) yields zero friction whereas the second definition leads to [32]

$$\frac{F_K(v)}{N} = \frac{2\pi^2 \gamma v b^2}{[\omega^2(2\pi c) - (2\pi v)^2]^2 + (2\pi v\gamma)^2}. \tag{22}$$

This result is *quadratic* in b because (8) is quadratic in ξ. To get the same result with (7) one has to calculate ξ_j up to second order in b (see appendix B).

For $v \to 0$ the kinetic friction (22) goes to zero. Thus we have the frictionless case $b < b_c^K$ from Sec. III A. For $c = 1$ we recover in leading order of b the exact result (A3). The solution (22) increases with v, reaching the maximum

$$\frac{F_K}{N} = \frac{b^2}{2\gamma v_1} + \mathcal{O}(\gamma) \tag{23}$$

at

$$v = v_1^S \equiv \frac{\omega(2\pi c)}{2\pi} + \mathcal{O}(\gamma^2) \tag{24}$$

and decreases to zero like $1/v^3$ for $v \to \infty$. The resonance peak occurs at that washboard frequency $2\pi v$ which corresponds to the frequency of the phonon having the same wave vector as the washboard wave.

Qualitatively the same behavior of the kinetic friction as a function of the sliding velocity is often found in dry friction experiments between atomically flat surfaces with a few mono-layers of lubricating molecules in between [4]. Usually such friction curves are interpreted as a dynamic phase transition from liquid-like behavior at small velocities to a solid-like state at high velocities. At the maximum of the kinetic friction the lubrication layer is assumed to be in an amorphous state [4,33].

We can give an estimate of the validity of the kinetic friction (22). The linearized equation of motion works fine as long as $|\xi_j| \ll 1$. Using (21) we find

$$b^2 \ll [\omega^2(2\pi c) - (2\pi v)^2]^2 + (2\pi v\gamma)^2. \tag{25}$$

The approximation (22) first fails at the resonance peak. Thus (23) is a good approximation as long as $b \ll \omega(2\pi c)\gamma$. For sliding velocities much larger than $\sqrt{b}/(2\pi)$ the approximation is always good because the particles make only tiny oscillations around their equilibrium positions. We call this state the *solid-sliding state*.

2. Superharmonic resonances

The last term in (17) is responsible for resonances of higher harmonics. For example, the solution (20) would lead to a term of the form

$$e^{4\pi i(vt+cj)}.$$

It is therefore natural to expand ξ_j into a Fourier series:

$$\xi_j = \sum_{m=-\infty}^{\infty} A_m e^{2\pi i m(vt+cj)}, \quad A_{-m} = A_m^*. \tag{26}$$

The linearized equation of motion turns into a set of linear algebraic equations for the Fourier coefficients A_m:

$$L_m A_m - \pi b(A_{m-1} + A_{m+1}) = \frac{ib}{2} (\delta_{m,-1} - \delta_{m,1}), \tag{27}$$

where $\delta_{i,j}$ is the Kronecker symbol and

$$L_m \equiv \omega^2(2\pi cm) - (2\pi vm)^2 + 2\pi vm\gamma\, i. \tag{28}$$

For small values of b, (27) can be solved perturbatively (see appendix B). In order to express F_K in terms of the Fourier components A_m, we use again definition (8) of the kinetic friction [32]:

$$\frac{F_K}{N} = 8\pi^2 \gamma v \sum_{m=1}^{\infty} |mA_m|^2. \tag{29}$$

Because A_m is proportional to $1/L_m$ we expect a peak in $F_K(v)$ near the *superharmonic resonance velocity*

$$v_m^S \equiv \frac{\omega(2\pi cm)}{2\pi m}. \tag{30}$$

This justifies an approximation of F_K which takes only the leading term in the power series of A_m into account:

$$\frac{F_K}{N} \approx 2v\gamma \sum_{m=1}^{\infty} m^2 \prod_{j=1}^{m} \left| \frac{\pi b}{L_j} \right|^2 . \qquad (31)$$

This is not a correct expansion of F_K in powers of b but it reproduces the superharmonic resonance peaks qualitatively very well as is shown in figure 4(a). It also gives the right scaling of the height of the resonance peaks, namely, b^{2m} for the superharmonic resonance of order m.

A special case of superharmonic resonance is $m = 1$ which is the main resonances. It can be shown that

$$v_1^S > v_m^S, \quad \text{for} \quad m > 1. \qquad (32)$$

Thus the superharmonic resonance peaks occur between zero and v_1^S. But they do not order sequentially (i.e., $v_n^S < v_m^S$ for some $n > m$) even though $v_m^S \to 0$ for $m \to \infty$.

3. Parametric resonances

The last term in the linearized equation of motion (17) is also responsible for parametric resonance of phonons. Parametric resonance is an instability phenomenon. The prototype is a pendulum with a vertically oscillating support [34]. The linearized equation of motion is the well-known Mathieu equation [35] which is a (damped) oscillator with eigenfrequency ω_0. Energy can be put into the oscillator due to periodic modulation (with frequency ω) of a parameter which determines ω_0. If the oscillator is damped this energy will dissipate.

The behavior of such a parametrically driven oscillator is very different from an oscillator which is driven by an additive force. In the latter case the response is linear whereas in the first case it is strongly nonlinear. The linear relationship between the amplitude of the oscillation and the strength of an additive force is caused by the fact that the driving force is *independent* of the amplitude of the oscillation whereas in a parametrically driven oscillator the force is proportional to the amplitude. This leads to a positive feedback mechanism. For a small proportionality constant (i.e., strength of driving) more energy is dissipated than is gained from driving and the oscillation dies out. But if the strength of driving exceeds a

certain threshold, more energy is gained than is dissipated and the amplitude increases. In a linear equation like the Mathieu equation such solutions go to infinity. But in real systems like the pendulum, nonlinearities will eventually saturate this growth.

The threshold for parametric resonance is a function on the frequency ratio ω_0/ω. It has relative minima near the *parametric resonance condition*

$$\omega = \frac{2\omega_0}{m}, \quad m = 1, 2, \ldots \tag{33}$$

where m denotes the order. The main difference between a parametrically driven oscillator and the FKT model is that in the latter case there are several oscillators (i.e. phonons), and the driving is spatially non-uniform because it is a wave. In this case the parametric resonance condition reads (see appendix B)

$$v_m^P(q) = \frac{\omega(\pi cm + q) + \omega(\pi cm - q)}{2\pi m}, \quad m = 1, 2, \ldots \tag{34}$$

This condition can be intuitively understood by the following picture: The linear chain is driven by the washboard wave which has "momentum" (i.e., wave number) $2\pi c$ and "energy" (i.e., frequency) $2\pi v$. If the driving is sufficiently strong, phonons with wave number $k_{\pm} = \pi cm \pm q$ are excited parametrically by m washboard waves. The condition (34) follows from the conservation laws of momentum and energy. It depends on a continuous parameter q contrary to the resonance condition (30). Of course the periodic boundary condition (2) restrict the value of q to N different values corresponding to N pairs of phonons. For $c = 1$ the driving is uniform and (34) becomes identical to (33) where ω_0 is the frequency of the pair of phonons with the same wave number but propagating in opposite directions and forming a standing wave. For weak damping the threshold for the m-th order parametric resonance is proportional to $\gamma^{1/m}$ (see in appendix B).

The maxima and minima of $v_m^P(q)$ define resonance intervals which successively appear for increasing b starting with the first-order parametric resonance. There is a relation between these instability intervals and the superharmonic resonances:

$$v_m^P \geq v_m^S. \tag{35}$$

Thus the first-order parametric resonance occurs for sliding velocities larger than the velocity v_1^S of the main resonance. For $\kappa \to 0$ the minimum of v_m^P is given by v_m^S. It is possible that

a superharmonic resonance peak sits in a parametric resonance interval, i.e., $\min v_m^P \leq v_n^S \leq \max v_m^P$ for $n \neq m > 1$. Also overlaps of instability intervals are possible.

For sliding velocities in an instability interval, the amplitudes of two phonons which are selected by $v = v_m^P$ increases exponentially. This exponential increase is saturated by the nonlinear terms omitted in (17). Their effects will be discussed in the following subsections. The increase and saturation of the amplitudes also occur in F_K. We expect that parametric resonance does not lead to a peak in $F_K(v)$ but to something which looks like a more or less flat table mountain. Furthermore, we expect quasiperiodic motion because the phonon frequencies $\omega(\pi cm + q)$ and $\omega(\pi cm - q)$ are in general incommensurate except for $c = 1$.

B. Periodic and quasiperiodic solutions

From section II A we know that the nonlinear equation of motion (5) is invariant under discrete translation in time. Solutions with the same symmetry should therefore exist. They can be described by a one-parameter function called *dynamical hull function* g_D:

$$\xi_j(t) = g_D(vt + cj), \quad \text{with} \quad g_D(x + 1) = g_D(x). \tag{36}$$

The dynamical hull function is very similar to the static hull function g_S introduced in Ref. [5]. In fact for $v \to 0$ the dynamical hull function becomes identical to the static one. It is a solution of

$$v^2 g_D''(x) + \gamma v g_D'(x) = g_D(x - c) + g_D(x + c) -$$
$$-(2 + \kappa)g_D(x) +$$
$$+b \sin 2\pi[x + g_D(x)]. \tag{37}$$

With the Fourier ansatz

$$g_D(x) = \sum_{m=-\infty}^{\infty} A_m e^{2\pi imx}, \quad A_{-m} = A_m^*. \tag{38}$$

this differential-delay equation turns into a set of nonlinear algebraic equations:

$$L_m A_m = b \int_0^1 \sin\left(2\pi x + 2\pi \sum_{l=-\infty}^{\infty} A_l e^{2\pi ilx}\right) e^{-2\pi imx} dx. \tag{39}$$

We solve this equation numerically by truncating the number of Fourier coefficients. Figure 4(b) shows the result for an increasing sequence of values of b.

We see that the dynamical hull function is not uniquely defined if b exceeds some threshold. The resonance peaks starting with the main resonance develop loops leading to bistability and hystereses. This is caused by the fact that the oscillation amplitude of the particle becomes of the same order as the periodicity of the external potential. These loops are also found in a single Tomlinson oscillator [10,11].

The nonlinear terms lead also to a reduction of the height of the resonance peaks compared to what is expected from the linear theory [see e.g. Fig. 4(a)]. Because the peak height in the linear theory is proportional to the inverse damping constant [see (23)], we interpret this result as an increase of the effective damping constant. The reason for this increase is the opening of additional channels of energy dissipation due to nonlinear phonon coupling.

In order to investigate the stability of the solution described by the dynamical hull function, one has to study the equation of motion linearized around (36). That is, we consider only those terms which are linear in $\delta\xi_j \equiv \xi_j - g_D(vt + cj)$. We get

$$\delta\ddot{\xi}_j + v\delta\dot{\xi}_j = \delta\xi_{j+1} + \delta\xi_{j+1} - (2 + \kappa)\delta\xi_j +$$
$$+ 2\pi b\cos(2\pi[vt + cj + g_D(vt + cj)])\,\delta\xi_j. \tag{40}$$

With the help of the well-known Floquet-Bloch ansatz for $\delta\xi_j$ (see appendix B) we solve this equation numerically with truncated Fourier expansions of g_D and $\delta\xi_j$.

There are two types of instabilities of the hull function. The first type is caused by the bistability of the resonance loop because there is always a separating unstable solution between the stable ones (called a saddle in the terminology of bifurcation theory). The other instability type is caused by parametric resonance already discussed for the linearized equation of motion (17) in Sec. IV A 3. From the stability analysis in appendix B we know that the most destabilizing disturbance contains two generically incommensurable frequencies ($2\pi v$ and Ω). This is confirmed numerically for (40). At these instabilities the system selects a state which leads most often to an enhanced kinetic friction. An example for this enhancement is shown in Fig. 4(c). The most prominent enhancement occurs for first-order

parametric resonance.

Figure 5(a) shows the quasiperiodic motion expected from Sec. IV A 3. It shows a stroboscopic map of the lateral force in time steps given the ratio of the lattice constant of the external potential divided by the velocity. The lateral force is given by

$$f_n \equiv -\frac{\kappa}{N} \sum_{j=1}^{N} \xi_j(n/v).$$

The dynamical hull function corresponds to a fixed point of the map

$$f_{n+1} = T(f_n).$$

Quasiperiodic motion leads to a closed one-dimensional attractor of the map. For $c = 1$ the motion is periodic leading to a limit cycle of period two.

C. Irregular behavior

For increasing driving strength b the quasiperiodic solutions caused by parametric resonance becomes unstable and the motion become more and more irregular and chaotic [see Fig. 5(b)]. It is presumably spatio-temporally chaotic as in the Frenkel-Kontorova model [36]. That is, the number of positive Lyapunov exponents is an extensive quantity [37], i.e., it is proportional to N. We call this strongly mixing state a *fluid-sliding state* even though the harmonic interaction in the model excludes on average changes in the particle order. Nevertheless the state is fluid-like because the amplitudes of the particle motion are of the same order as the lattice constant c.

The kinetic friction F_K from simulations are shown in Figure 6. In each simulation the sliding velocity was increased in tiny steps from zero up to a certain value and then decreased back to zero. Beyond first-order parametric resonance (i.e., $v > \max v_1^P$) large hysteresis loops occur leading to bistability between fluid-sliding states and the solid-sliding state.

Characteristic peaks appear in $F_K(v)$ in the regime of fluid-sliding states beyond the main resonance. What is the nature of these peaks? Looking at the spatially and temporally resolved dynamics we were not able to see any difference between the dynamics inside and outside the peaks. The motion is strongly irregular. The only exceptions are the large peaks

at $v = 1.06$ and $v = 0.95$ for $c = 144/233$ and $c = 1$, respectively. Here coherent motion appears which is investigated in the following subsection.

The spatio-temporal Fourier transformation of $\xi_j(t)$ reveals a structured distribution in the (wave-number, frequency) space which is mostly concentrated on the curve defined by the dispersion relation (18). Therefore the strongly chaotic motion in the fluid-sliding state is mainly caused by weak nonlinear interactions between phonons.

Here we will give only some qualitative arguments for the occurrence of the peaks beyond the main resonance. The argument is based on the picture of multi-phonon scattering processes already used in subsection IV A to explain parametric resonance. The most general process which drives the phonon system is the decay of m washboard waves into n different phonons. From energy and momentum conservation we get

$$v = v_m^n \equiv \frac{\sum_{j=1}^{n} \omega(k_j)}{2\pi m} \tag{41a}$$

and

$$2\pi(cm + u) = \sum_{j=1}^{n} k_j, \quad \text{with } u \text{ integer.} \tag{41b}$$

The integer u denotes possible Umklapp processes. The strength of the decay processes scales like b^m. The most important processes are those with small n and m. Superharmonic resonance (i.e., $n = 1$) and parametric resonance (i.e., $n = 2$) are the linear cases. For $n > 2$ the decay processes are nonlinear. Beyond first-order parametric resonance (i.e., $v > \max v_1^P$) the solid-sliding state is therefore insensitive to these processes. They become active only if at least some phonons are excited. Then they excite additional phonons leading, to a self-sustained process that converts macroscopic, uniform sliding into microscopic, irregular motion.

An important quantity characterizing the efficiency of phonon driving due to washboard waves is the density of combinations of wave vectors fulfilling (41) for sliding velocities from the interval of $[v, v + dv]$. We call this density the *density of decay channels*. We expect that characteristic structures of this density, such as peaks, also appear in $F_K(v)$.

Because of the constant wave-number density due to periodic boundary conditions, the density of decay channels of an n-wave decay process of order m reads

$$\rho_m^n(v) = \frac{1}{(2\pi)^{n-1}} \int\limits_0^{2\pi} \cdots \int\limits_0^{2\pi} \delta(v - v_m^n) \, dk_1 \ldots dk_{n-1}, \tag{42}$$

where δ is Dirac's delta function and k_n in v_m^n is substituted due to (41b).

TABLES

TABLE I. The extrema of the main decay processes for $\kappa = 1$, $m = 1$, and (a) $c = (\sqrt{5} - 1)/2$ and (b) $c = 1$. p and $n-p$ are the number of phonons having wave number k_- and k_+, respectively.

(a)

n	v_m^n	p	k_-	k_+	Type
2	0.4800	1	5.4049	4.7615	minimum
2	0.4801	0		5.0832	maximum
2	0.6143	0		1.9416	maximum
3	0.6052	0		5.4832	minimum
3	0.7475	1	0.9028	1.4902	saddle
3	0.7480	0		1.2944	maximum
3	1.0611	0		3.3888	maximum
4	0.7395	0		5.6832	minimum
4	0.8707	0		0.9708	minimum
4	0.8734	1	1.7615	0.7072	saddle
4	1.2191	1	6.1524	3.4324	saddle
4	1.2936	0		4.1124	maximum
4	1.3729	0		2.5416	maximum

(b)

n	v_m^n	p	k_-	k_+	Type
2	0.3183	0		0.0000	minimum
2	0.7118	0		3.1416	maximum
3	0.4775	0		0.0000	minimum
3	0.8709	1	0.0000	3.1416	saddle
3	0.9549	0		2.0944	maximum
4	0.6366	0		0.0000	minimum
4	1.0300	2	0.0000	3.1416	saddle
4	1.0950	1	0.6283	1.8850	saddle
4	1.1027	0		1.5708	maximum
4	1.4235	0		3.1416	maximum

Extrema of v_m^n lead to singularities in ρ_m^n which are generalizations of van-Hove singularities well-known from phonon spectra [38]. In appendix C we have calculated the extrema. For the parameters of Fig. 6 the most important extrema are tabulated in table I. The scaling behavior of ρ_m^n near an extremum depends on its type. The most prominent singularities are the diverging ones. There are two cases of diverging singularities. The first one occurs only for $n = 2$ where the density scales like $|v - v_c|^{-1/2}$ near maxima and minima of v_m^n. For $n > 2$ logarithmic singularities occur near certain types of saddles. A saddle can be characterized by the numbers n_+ and n_- which count the linearly independent directions in which v_m^n increases or decreases, respectively. Logarithmic singularities occur only if both numbers are odd (see appendix D).

For the parameters of Fig. 6 we have calculated numerically the density ρ_m^n of the most important decay processes. The results are shown in figure 7. Together with table I we are able to identify all peaks in $F_K(v)$ that occur beyond the main resonance.

Concerning the strength of friction this is only a qualitative analysis. The reason for that is twofold. First, the decay channels are not equally fed and, second, we do not know the effective damping constant of the phonon modes due to nonlinear phonon scattering. This information would be needed in order to obtain a quantitative theory of $F_K(v)$.

D. Coherent motions and solitons

As already mentioned in the previous subsection, the motion is not entirely chaotic near the large peaks at $v = 1.06$ and $v = 0.95$ for $c = 144/233$ and $c = 1$, respectively. Coherent waves occur, as can be seen in Figure 8. A spatio-temporal Fourier analysis shows a peak which does not sit on the dispersion relation but near the point which is determined by the wave number and frequency of the phonon of the decay process that belongs to the absolute maximum of v_1^3.

In the example shown in Fig. 8 we observe a modulation of the amplitude of the fast oscillation. We have extracted the amplitude of this envelope from the data of the simulation. Figure 9 shows the spatio-temporal evolution of this amplitude. The regular motion of the equidistant maxima of the envelope in Fig. 8 appears as parallel white stripes in Fig. 9.

On this background pattern three dark stripes are visible. They are a kind of *dark solitons* well-known from the nonlinear Schrödinger equation. Since they propagate with different velocities, collisions occur which are nondestructive like in the nonlinear Schrödinger equation. Thus the FKT model seems to behave like a conservative, undamped and undriven system. But the waves emitted by the solitons are strongly damped.

V. CONCLUSION

We have studied the dynamical properties of the FKT model driven at a constant sliding velocity v. The model describes in a rudimentary way the interface between two atomically flat sliding surfaces. An advantage of this model is that some basic questions concerning dry friction can be studied analytically.

Since dry friction operates mostly far from equilibrium, we are in principle not able to calculate macroscopic properties by using straightforward recipes. In the sliding process of two solids, the uniform motion is turned into microscopic, irregular motion called heat. The rate of dissipation determines the kinetic friction F_K. What are the mechanisms of this transfer from macroscopic to microscopic motion? How effective are these mechanisms?

The two basic dissipation channels in the FKT model are the damping terms which are proportional to the velocities of the interface particles relative to the sliding bodies. The basic mechanisms of energy transfer are multi-phonon decay processes where m so-called washboard waves excite n phonons of the chain of interface particles. The washboard is the spatially periodic potential describing the atomically flat surface of the lower body. It acts as a wave (wave length = surface lattice constant, frequency = sliding velocity divided by wave length) in the frame of the upper body to which the surface particles are connected by springs. The washboard is driving the surface particles. For small driving strength b and large damping the process with $m = 1$ and $n = 1$ is the most dominant one. It simply leads to a resonance peak in the kinetic friction $F_K(v)$ given by (22). A broad peak is exactly what is found in boundary lubrication [33]. For large velocities the washboard shakes the particles so rapidly that its influence is averaged out. Therefore the interaction becomes effectively zero. The interface motion freezes out forming the solid-sliding state. In this

state the kinetic friction is proportional to the sliding velocity. Note that in Figs. 4 and 6 this part of the kinetic friction is always omitted.

For increasing b or decreasing damping superharmonic resonance peaks occur. They are caused by processes with $m > 1$ and $n = 1$. The superharmonic resonance peaks are smaller than the main resonance peak and occur for velocities below the main resonance. As long as the oscillation amplitudes of the interface particles are much less than the washboard wave-length, the main resonance and superharmonic resonances can by approximated analytically very well from the linearized equation of motion. Otherwise processes with $n > 1$ become important leading to nonlinear phonon damping. This increases the effective damping constant resulting in a decrease of the resonance peaks in accordance with (23).

The decay process with $m = 1$ and $n = 2$ is responsible for an instability (first-order parametric resonance) of the solid-sliding state if b exceeds some threshold which is proportional to the damping constant. This instability occurs for a whole interval of v beyond main resonance. The amplitudes of both phonons increase. Nonlinearities in the equation of motion eventually saturate the growth due to nonlinear phonon damping. This leads to quasiperiodic motion because the phonon frequencies are in general incommensurate. The kinetic friction in the parametric resonance window can be larger than at the main resonance.

A further increase of b leads to bistability between the solid-sliding state and the so-called fluid-sliding state which is characterized by spatio-temporal chaos. The kinetic friction of this state exhibits some peaks which can be qualitatively understood by the density of decay channels for processes with $m = 1$ and $n = 2$, 3, and 4. In the regime of fluid-sliding states a small velocity interval is embedded where coherent motion including nondestructive collisions of dark envelope solitons occurs.

It should be noted that the behavior beyond main resonance does not depend on the commensurability of the ratio c of the surface lattice constants of the sliding bodies, contrary to what is found for small sliding velocities.

The behavior for small sliding velocities is dominated by stick-slip motion of the interface particles. In the overdamped limit every Q-th particle (Q is the denominator of c) jumps into the neighboring potential well leading to $F_S - F_K(v \to 0) \sim 1/Q$. Thus the kinetic friction $F_K(v \to 0)$ is identical with the static friction F_S in the incommensurate case. The

kinetic friction is proportional to the sliding velocity if $b < b_c^K$. In any case $F_K(v)$ is an increasing function at $v = 0$. For finite damping constants particles may jump to more distant potential wells leading to kinetic friction which is less than the kinetic friction in the overdamped limit. Furthermore, this stick-slip motion becomes more irregular.

In order to compare the dynamical behavior of the FKT model with the BK model we have to note that most studies at the BK model are done for $\kappa \ll 1$ whereas in our study we have always chosen $\kappa = 1$. The behavior of the BK model is different for $\kappa = 1$ compared to $\kappa \ll 1$. For example, the solitonic motion of a group of a few blocks found by Schmittbuhl et al. [20] disappears if κ is too large [22]. For $\kappa = 1.2$ Sarkadei and Jacobs [23] have found regular periodic waves. They travel from the open end into the chain and annihilate somewhere in the middle. But contrary to the FKT model, this behavior does not lead to resonance peaks in the kinetic friction [22,23]. The reason for that may be the fact that in the BK model energy is dissipated during the sticking phases of the blocks and not during sliding.

There are several theoretical studies [31,36,39–42] where the kinetic friction is investigated in a system which is driven by a constant force and not by a constant velocity as in our study of the FKT model. The averaged velocity of the center of mass is calculated. All these studies show fluid-sliding states with enhanced friction and solid-sliding states where the kinetic friction is given by the sliding velocity times the damping constant. Hysteresis between the solid-sliding state and fluid-sliding state occurs only if the temperature is small enough [42]. Therefore we expect that the strong hysteresis in the FKT model disappears for finite and large enough temperatures.

A model which goes beyond the FKT model has been studied by Sokoloff [9,29,43]. Instead of one layer it has several layers coupled harmonically. Thus the driving due to the washboard wave is no longer uniform. Sokoloff has calculated the kinetic friction analytically for a prescribed periodic motion of the layer which feels the periodic potential. The result is therefore similar our results for the main resonance and superharmonic resonance (if the prescribed motion has higher harmonics). This kind of approach is not able to deal with instabilities like parametric resonances or other multi-phonon processes. It would be worthwhile to study such an extension of the FKT model from our point of view.

In a forthcoming paper we will study macroscopic stick-slip motion of the FKT model by coupling the upper sliding body via a spring at a support which moves with constant velocity. We are interested in the following questions. What is the interplay between static friction and kinetic friction? What happens during the transitions from stick to slip and vice versa? Which (meta)stable states does the system select after the slip-to-stick transition?

ACKNOWLEDGMENTS

APPENDIX A: QUASISTATIC SLIDING IN THE TOMLINSON LIMIT AND FOR $c = 1$

In the Tomlinson limit (i.e., $\kappa, b \to \infty$) and for $c = 1$ the static hull function g_S can be given in parametric form because the next-neighbor coupling in (5) can be dropped: [5]

$$g_S(\tau) = \frac{b}{\kappa} \sin 2\pi\tau, \quad x(\tau) = \tau - g_S(\tau). \tag{A1}$$

In order to calculate F_K in the quasistatic limit $v \to 0$ we have to distinguish between $b < b_c^K = \kappa/(2\pi)$ and $b > b_c^K$.

In the first case we can apply (10) with γ_{eff} defined by (11). To do this the integral $\int_0^1 (dg_S/dx)^2 dx$ has to be calculated. Using (A1) we get

$$\int_0^1 \frac{(dg_S/d\tau)^2}{1 - dg_S/d\tau} d\tau = \frac{1}{\sqrt{1 - \left(\frac{2\pi b}{\kappa}\right)^2}} - 1. \tag{A2}$$

Thus

$$\gamma_{\text{eff}} = \gamma_L + \gamma \left(\frac{1}{\sqrt{1 - \left(\frac{2\pi b}{\kappa}\right)^2}} - 1 \right). \tag{A3}$$

For $b > b_c^K$ the hull function g_S is no longer a unique function of x. There is a saddle-node bifurcation at the relative maximum of $x(\tau)$ at

$$2\pi\tau_{SN} = \arccos \frac{\kappa}{2\pi b}. \tag{A4}$$

For the same value of x there is at least a second solution defining a τ_2 implicitly by

$$\tau_2 - g_S(\tau_2) = \tau_{SN} - g_S(\tau_{SN}). \tag{A5}$$

This equation can be solved perturbatively near $b = b_c^K$ and $\kappa/b \to 0$ leading to

$$2\pi\tau_2 = 4\sqrt{\frac{\pi}{\kappa}(b - b_c^K)} - \frac{38}{15}\left(\frac{\pi}{\kappa}(b - b_c^K)\right)^{3/2} +$$
$$+ \frac{1037}{350}\left(\frac{\pi}{\kappa}(b - b_c^K)\right)^{5/2} + \mathcal{O}((b - b_c^K)^{7/2}) \tag{A6}$$

and

$$2\pi\tau_2 = 2\pi n - \frac{\pi}{2} - \sqrt{\frac{2n\kappa}{b}} + \frac{\kappa}{2\pi b} - \frac{1}{3}\left(\frac{n\kappa}{2b}\right)^{3/2} +$$
$$+ \frac{n}{6\pi}\left(\frac{\kappa}{b}\right)^2 + \mathcal{O}((\kappa/b)^{5/2}), \tag{A7}$$

with $n = 1, 2, \ldots$, respectively.

Because x corresponds to the relative position of the sliding bodies, an increase of x beyond the relative maximum yields a jump of one particle into a state corresponding to the solution of (A5). In order to calculate the kinetic friction it is most convenient to investigate the difference of the potential energy before and after the jump:

$$\Delta V = \frac{b}{2\pi}[\cos 2\pi\tau_{SN} - \cos 2\pi\tau_2] +$$
$$+ \frac{\kappa}{2}[g_S(\tau_{SN})^2 - g_S(\tau_2)]. \tag{A8}$$

This expression can be simplified by using (A1) and (A4):

$$\Delta V = \frac{\kappa}{8\pi^2}\left(1 - \frac{2\pi b}{\kappa}\cos 2\pi\tau_2\right)^2. \tag{A9}$$

In accordance with (13) the kinetic friction reads

$$F_K(v \to 0) = \frac{\Delta V}{\langle n \rangle} N, \tag{A10}$$

where $\langle n \rangle$ is the number of potential wells a particle jumps on average. For $b \to b_c^K$ a particle can jump only into the next potential well. Thus $\langle n \rangle = 1$ and we get with (A6)

$$\frac{F_K(v \to 0)}{N} = \frac{9}{2\kappa}(b - b_c^K)^2 - \frac{36\pi}{5\kappa^2}(b - b_c^K)^3 +$$
$$+ \frac{2124\pi^2}{175\kappa^3}(b - b_c^K)^4 + \mathcal{O}((b - b_c^K)^5). \tag{A11}$$

In the limit $\kappa/b \to 0$ we get with (A7)

$$\frac{F_K(v \to 0)}{N} = b\left(1 - \frac{\langle n \rangle \kappa}{2b} + \right.$$
$$\left. + \frac{\sqrt{2\langle n \rangle}}{3\pi}\left(\frac{\kappa}{b}\right)^{3/2} + \mathcal{O}((\kappa/b)^2)\right). \tag{A12}$$

These equations generalize the results of Ref. [10].

APPENDIX B: PERTURBATION THEORY FOR THE LINEARIZED EQUATION OF MOTION

The linearized equation of motion (17) can be treated analytically in the framework of a perturbation theory with b as the smallness parameter.

First the solution is calculated in the following way. We start with (27) and expand the solution:

$$A_m = \sum_{l=1}^{\infty} A_{m,l} b^l. \tag{B1}$$

Inserting this ansatz into (27) leads to a recursion equation for the coefficients $A_{m,l}$:

$$A_{m,1} = \frac{i}{2L_m}(\delta_{m,-1} - \delta_{m,1}) \tag{B2}$$

and

$$A_{m,l+1} = \frac{\pi}{L_m}(A_{m+1,l} + A_{m-1,l}). \tag{B3}$$

The solution of this recursion scheme is

$$A_{m,l} = -\frac{i\pi^{l-1}}{2} \sum_{\substack{\sigma_1,\ldots,\sigma_l=-1 \\ \sum_{i=1}^{l} \sigma_i = m}}^{1} \sigma_1 \prod_{i=1}^{l} \frac{1}{L_{\sum_{j=1}^{i} \sigma_j}}. \tag{B4}$$

Thus the only nonzero coefficients are

$$A_{m,m+2n}, \quad \text{with} \quad m+n \neq 0, \; m,n = 0, 1, \ldots \tag{B5}$$

Therefore the leading term of the Fourier component A_m is of order b^m:

$$A_m = -\frac{i(\pi b)^m}{2\pi} \left(\prod_{i=1}^{m} \frac{1}{L_i}\right) \times$$

$$\times \left(1 - \frac{(\pi b)^2}{L_{-1}L_0} + \sum_{k=0}^{m} \frac{(\pi b)^2}{L_k L_{k+1}} + \mathcal{O}(b^4)\right) \tag{B6}$$

Using (29) we get for the kinetic friction

$$\frac{F_K}{N} = 8\pi^2 v\gamma \sum_{l=1}^{\infty} b^{2l} \sum_{m=1}^{l} m^2 \sum_{n=0}^{l-m} A_{m,m+2n} A^*_{m,2l-m-2n}, \tag{B7}$$

which is an even function in b as expected from symmetry.

In order to study the stability of the solutions of (17), we make the following ansatz in accordance with the well-known Floquet-Bloch theorem :

$$\xi_j = \sum_{m=-\infty}^{\infty} a_m e^{2\pi i m(vt+cj)+iqj+\lambda t}, \tag{B8}$$

where q is an arbitrary given wave number (with qN an integer multiple of 2π) and λ a complex number which is an eigenvalue of:

$$D_m a_m - \pi b(a_{m-1} + a_{m+1}) = 0, \tag{B9}$$

with

$$D_m = (2\pi i v m + \lambda)^2 + \gamma(2\pi i v m + \lambda) + \omega^2(2\pi cm + q). \tag{B10}$$

Note that (B9) is invariant under the transformation $\lambda \to \lambda+2\pi iv$, $q \to q+2\pi c$, $a_m \to a_{m+1}$. A solution of (17) is stable as long as the real parts of all eigenvalues are negative. In order to calculate the instability threshold b_c it is more convenient to solve (B9) for $\lambda = i\Omega$ where b and Ω are the unknown variables. The diagonal elements turn into

$$D_m = R_m + i\gamma I_m, \tag{B11}$$

with

$$R_m = \omega^2(2\pi cm + q) - I_m^2, \quad I_m = 2\pi vm + \Omega. \tag{B12}$$

The real solution b of (B9) with the smallest absolute value defines a function of q. Its absolute minimum gives the instability threshold b_c. It is always zero in the undamped case (i.e., $\gamma = 0$) because at least one D_m is zero. In the case of damping all D_m's are nonzero.

Parametric resonance of order n corresponds to the fact that two diagonal elements, say D_0 and D_n, go to zero for $b \to 0$ and $\gamma \to 0$. In order to calculate the instability threshold we assume that a_0 and a_n are given. Next we express $a_{\pm 1}$ and $a_{n \pm 1}$ in terms of a_0 and a_n:

$$a_{-1} = -\frac{\pi b \, d_{-\infty}^{-2}}{d_{-\infty}^{-1}} a_0, \tag{B13}$$

$$a_1 = -\frac{\pi b \, d_2^{n-1}}{d_1^{n-1}} a_0 - \frac{(-1)^n (\pi b)^{n-1}}{d_1^{n-1}} a_n, \tag{B14}$$

$$a_{n-1} = -\frac{\pi b \, d_1^{n-2}}{d_1^{n-1}} a_n - \frac{(-1)^n (\pi b)^{n-1}}{d_1^{n-1}} a_0, \tag{B15}$$

$$a_{n+1} = -\frac{\pi b \, d_{n+2}^{\infty}}{d_{n+1}^{\infty}} a_n, \tag{B16}$$

where

$$d_n^m = \begin{vmatrix} D_n & \pi b & & 0 \\ \pi b & D_{n+1} & \ddots & \\ & \ddots & \ddots & \pi b \\ 0 & & \pi b & D_m \end{vmatrix}. \tag{B17}$$

Eq. (B9) for $m = 0$ and $m = n$ turns into a set of linear equations for a_0 and a_n. It has nontrivial solutions if the determinant

$$\begin{vmatrix} \dfrac{D_0}{(\pi b)^2} - \dfrac{d_{-\infty}^{-2}}{d_{-\infty}^{-1}} - \dfrac{d_2^{n-1}}{d_1^{n-1}} & -(-1)^n \dfrac{(\pi b)^{n-2}}{d_1^{n-1}} \\[2ex] -(-1)^n \dfrac{(\pi b)^{n-2}}{d_1^{n-1}} & \dfrac{D_n}{(\pi b)^2} - \dfrac{d_{n+2}^{\infty}}{d_{n+1}^{\infty}} - \dfrac{d_1^{n-2}}{d_1^{n-1}} \end{vmatrix} \tag{B18}$$

is zero. The assumption

$$R_0, R_n = \mathcal{O}(b^2), \quad R_m = \mathcal{O}(b^0), \; m \neq 0, n, \tag{B19}$$

yields

$$\left(\prod_{m=1}^{n-1} D_j + \mathcal{O}(b^2) \right)^2 \left[-\gamma^2 I_0 I_n + \mathcal{O}(b^2) \right] = (\pi b)^{2n}. \tag{B20}$$

Thus in leading order of γ we obtain

$$\pi b_c = \left(\gamma \sqrt{-I_0 I_n} \prod_{m=1}^{n-1} |R_j| \right)^{1/n}. \tag{B21}$$

The product term does not appear for $n = 1$. Bearing in mind that $I_0 I_n$ has to be negative and $\omega(k)$ is an even function we immediately get the parametric resonance condition (34) by solving $R_0 = R_n = 0$.

APPENDIX C: EXTREMA OF v_m^n

Before calculating the extrema of v_m^n defined by (41) we eliminate k_n by using (41b). Thus v_m^n is a function of $k_1, \ldots, k_{n-1}$. An extremum is given by

$$2\pi m \partial_{k_j} v_m^n = \omega'(k_j) - \omega'(k_n) = 0, \quad j = 1, \ldots, n-1, \tag{C1}$$

where

$$\omega'(k) = \frac{d\omega}{dk} = \frac{\sin k}{\omega(k)} \tag{C2}$$

is the derivative of the dispersion relation (18). For an extremum all $\omega'(k_j)$ have to be the same. Because $\omega'(k)$ is a periodic function, there exist two solutions k_- and k_+ in the interval $[-\pi, \pi)$. For a given value of k_+ we can calculate the corresponding k_- by solving $\omega'(k_-) = \omega'(k_+)$:

$$k_- = \text{sign}\,(k_+) \arccos\left(\frac{2 - (\kappa + 2)\cos k_+}{\kappa + 2 - 2\cos k_+}\right), \tag{C3}$$

where sign is the signum function. Therefore an extremum is given by

$$v_m^n = \frac{p\omega(k_-) + (n - p)\omega(k_+)}{2\pi m}, \tag{C4}$$

where p and $n - p$ are the numbers of wave vectors which have the wave numbers k_- and k_+, respectively.

The wave number k_- is not arbitrary because momentum conservation (41b) has to be satisfied:

$$pk_- + (n - p)k_+ = 2\pi(mc + u), \quad \text{with } u \text{ integer.} \tag{C5}$$

Eliminating k_- in (C5) by using (C3) leads to a nonlinear algebraic equation for k_+ which can be solved only numerically except for $p = 0$. In this case all wave vectors are identical. That is,

$$k_j = k_+ = 2\pi \frac{mc + u}{n}, \quad j = 1, \ldots, n. \tag{C6}$$

The type of the extremum is determined by the eigenvalues of

$$2\pi m \partial_{k_j} \partial_{k_l} v_m^n = \omega''(k_j)\delta_{j,l} + \omega''(k_n), \tag{C7}$$

where $\omega''(k)$ is the second derivative of the dispersion relation (18). For $p = 0$ the eigenvalues are

$$\lambda_1 = n\omega''(k_+), \quad \lambda_j = \omega''(k_+), \quad j = 2, \ldots, n-1. \tag{C8}$$

Thus the extremum is either a maximum or minimum depending on the sign of ω''. In the general case we have two eigenvalues given by

$$\lambda = \frac{\omega''_- + n\omega''_+ \pm \sqrt{(\omega''_- - n\omega''_+)^2 + 4p\omega''_+(\omega''_- - \omega''_+)}}{2}, \tag{C9}$$

where

$$\omega''_\pm \equiv \omega''(k_\pm), \tag{C10}$$

$p - 1$ times the eigenvalue $\lambda = \omega''_-$, and $n - p - 2$ times the eigenvalue $\lambda = \omega''_+$.

APPENDIX D: SCALING OF ρ_m^n NEAR EXTREMA OF v_m^n

The scaling behavior of ρ_m^n near an extremum of $v_m^n(k_1, \ldots, k_{n-1})$ can be easily obtained after a linear transformation of the coordinate system $k_1, \ldots, k_{n-1}$ into a new system $x_1, \ldots, x_{n-1}$ which is given by the eigendirections of the matrix defined by the second derivatives of v_m^n calculated at the extremum. Up to second order we get

$$v_m^n = v_c + \sum_{j=1}^{n_+} x_j^2 - \sum_{j=1}^{n_-} x_j^2, \tag{D1}$$

where n_+ (n_-) is the number of positive (negative) eigenvalues of that matrix. A non-singular matrix leads to $n_+ + n_- = n - 1$, otherwise $n_+ + n_- < n - 1$.

The scaling behavior near an extremum is determined by the states nearby. Thus we perform the integration (42) only in a spherical domain of radius R:

$$\rho_m^n \sim \int_0^R \int_0^R \delta(v - v_c - r_+^2 + r_-^2) r_+^{n_+ - 1} r_-^{n_- - 1} dr_+ dr_-, \tag{D2}$$

where $r_\pm^2 \equiv \sum_{j=1}^{n_\pm} x_j^2$. One integration yields

$$\rho_m^n \sim \int_0^R (v - v_c - r_-^2)^{n_+/2 - 1} r_-^{n_- - 1} dr_-. \tag{D3}$$

In the case of either a relative minimum or maximum (i.e., $n_- = 0$ or $n_+ = 0$) we get therefore

$$\rho_m^n \sim (v - v_c)^{n_+/2-1} \quad \text{or} \quad \rho_m^n \sim (v_c - v)^{n_-/2-1}. \tag{D4}$$

In the case of a saddle (i.e., $n_\pm \neq 0$) we perform the second integration (D3) by using the Euler substitution

$$t = r_- + \sqrt{z + r_-^2}, \quad \text{with} \quad z \equiv v - v_c,$$

which yields

$$\rho_m^n \sim \int\limits_{\sqrt{z}}^{\sqrt{z+R^2}+R} (t^2 + z)^{n_+-1}(t^2 - z)^{n_--1} t^{1-n_+-n_-} dt. \tag{D5}$$

Neglecting the contribution from the upper limit we get

$$\rho_m^n \sim \sum_{j_+=0}^{n_+-1} \sum_{j_-=0}^{n_--1} (-1)^{j_-} \binom{n_+ - 1}{j_+} \binom{n_- - 1}{j_-} \times$$
$$\times z^{\frac{n_++n_-}{2}-1} I(n_+ - n_- - 2 - 2j_+ - 2j_-), \tag{D6}$$

where

$$I(s) \equiv \begin{cases} \ln z, & s = 0 \\ 1, & s \neq 0 \end{cases}. \tag{D7}$$

The logarithmic term appears only if

$$C \equiv \sum_{\substack{j_\pm=0 \\ 2(j_++j_-+1)=n_++n_-}}^{n_\pm-1} (-1)^{j_-} \binom{n_+ - 1}{j_+} \binom{n_- - 1}{j_-} \tag{D8}$$

is not zero. It is easy to show that $C = -(-1)^{n_\pm}C$ holds. Thus

$$\rho_m^n \sim |v - v_c|^{\frac{n_++n_-}{2}-1} \begin{cases} \ln |v - v_c|, & n_\pm \text{ are odd} \\ 1, & \text{otherwise} \end{cases}. \tag{D9}$$

REFERENCES

* Present Address: Institut für Angewandet Physik, Universität Bern, Sidlerstr. 5, CH-3012 Bern, Switzerland.

[1] F. P. Bowden and D. Tabor, *Friction and Lubrication* (Oxford University Press, 1954).

[2] I. L. Singer and H. M. Pollock (eds), *Fundamentals of friction: macroscopic and microscopic processes* (Kluwer Academic Publishers, Dordrecht, 1992).

[3] F. Heslot, T. Baumberger, B. Perrin, B. Caroli, and C. Caroli, Phys. Rev. E **49**, 4973 (1994).

[4] B. Bhushan, J. N. Israelachvili, and U. Landman, Nature **374**, 607 (1995).

[5] M. Weiss and F. J. Elmer, Phys. Rev. B **53**, 7539 (1996).

[6] G. A. Tomlinson, Phil. Mag. Series 7, **7**, 905 (1929).

[7] G. M. McClelland, in *Adhesion and Friction*, M. Grunze and H.J. Kreuzer (eds.), Springer Series in Surface Science **17**, 1 (Springer Verlag, Berlin, 1990).

[8] G. M. McClelland and J. N. Glosli, in Ref. [2], p. 405.

[9] J. B. Sokoloff, Surf. Sci. **144**, 267 (1984).

[10] J. S. Helman, W. Baltensberger, and J. A. Hołyst, Phys. Rev. B **49**, 3831 (1994).

[11] F. J. Elmer, Helv. Phys. Acta **67**, 213 (1994).

[12] In Ref. [10] also multiple resonances of the form $\omega = n\omega_0$, where n is an integer greater than two, are mentioned. But such resonances do not occur in the limit of disappearing interaction and dissipation. Therefore we believe that the occurrence of these resonances depends on the model.

[13] This is in contrast to the suggestion at the end of Ref. [10].

[14] M. Weiss and F. J. Elmer, in *The physics of sliding friction*, B. N. J. Persson and E. Tosatti (eds.), (Kluwer Academic Publishers, Dordrecht, 1996).

[15] R. Burridge and L. Knopoff, Bull. Seismol. Soc. Am. **57**, 341 (1967).

[16] J. M. Carlson and J. S. Langer, Phys. Rev. Lett. **62**, 2632 (1989), Phys. Rev. A **40**, 6470 (1989).

[17] J. M. Carlson, J. S. Langer, B. E. Shaw, and C. Tang, Phys. Rev. A **44** 884 (1991).

[18] G. L. Vasconcelos, M. de Sousa Vieira, and S. R. Nagel, Physica A **191**, 69 (1992).

[19] M. de Sousa Vieira, G. L. Vasconcelos, and S. R. Nagel, Phys. Rev. E **47**, R2221 (1993).

[20] J. Schmittbuhl, J.-P. Vilotte, and S. Roux, Europhys. Lett. **21**, 375 (1993).

[21] M. de Sousa Vieira and H. J. Herrmann, Phys. Rev. E **49**, 4534 (1994).

[22] P. Español, Phys. Rev. E **50**, 227 (1994).

[23] M. R. Sarkadei and R. L. Jacobs, Phys. Rev. E **51**, 1929 (1995).

[24] M. de Sousa Vieira, Phys. Rev. E. **54**, 5925 (1996).

[25] D.W. Heermann, *Computer Simulation Methods in Theoretical Physics*, Springer-Verlag (1986).

[26] This should not be confused with the fact that for the *undriven* FKT model, where the positions of the sliding bodies are *not* externally controlled, metastable states occur not before b exceeds a second threshold $b_c^m \geq b_c^K$ (for more details, see Ref. [5]).

[27] T. Gyalog, unpublished Diploma thesis, Universität Basel.

[28] F. J. Elmer, in *The physics of sliding friction*, B. N. J. Persson and E. Tosatti (eds.), (Kluwer Academic Publishers, Dordrecht, 1996).

[29] J.B. Sokoloff, Phys. Rev. B **42**, 760 (1990).

[30] B. N. J. Persson, J. Chem. Phys. **103**, 3849 (1995).

[31] B. N. J. Persson and A. Nitzan, Surf. Sci. **367**, 261 (1996).

[32] The first term of (8) is always dropped throughout Sec. IV.

[33] H. Yoshizawa and J. Israelachvili, J. Phys. Chem. **97**, 11300 (1993).

[34] L.D. Landau and L.M. Lifshitz, *Mechanics* (Pergamon Press, Oxford, 1976).

[35] M. Abromowitz and I.A. Stegun (eds.), *Handbook of Mathematical Functions* (Dover, New York, 1965).

[36] T. Strunz and F. J. Elmer, in *The physics of sliding friction*, B. N. J. Persson and E. Tosatti (eds.), (Kluwer Academic Publishers, Dordrecht, 1996).

[37] M. C. Cross and P. C. Hohenberg, Rev. Mod. Phys. **65**, 851 (1993).

[38] G. Weinreich, *Solids: Elementary Theory for Advanced Students* (Wiley, New York, 1965).

[39] B. N. J. Persson, Phys. Rev. B **48**, 18140 (1993).

[40] H. Matsukawa and H. Fukuyama, Phys. Rev. B **49**, 17286 (1994).

[41] E. Granato, M. R. Baldan, and S. C. Ying, in *The physics of sliding friction*, B. N. J. Persson and E. Tosatti (eds.), (Kluwer Academic Publishers, Dordrecht, 1996).

[42] O. M. Braun, T. Dauxois, M. V. Paliy, and M. Peyrard, preprint cond-mat/9701134.

[43] J.B. Sokoloff, J. Appl. Phys. **72**, 1262 (1992).

FIGURES

FIG. 1. A schematical sketch of the Frenkel-Kontorova-Tomlinson (FKT) model.

FIG. 2. The friction force in the limit of quasistatic sliding (i.e., $v \to 0$) for $\kappa = 1$. The solid lines show the kinetic friction F_K in the overdamped limit (i.e., $\gamma \to \infty$). The dashed lines denote the static friction F_S. $F_S^{max} = bN$ is the overall upper bound of static friction. For $c = 1$ the analytically obtained approximations of F_K, (A11) and (16), are shown by dotted lines.

FIG. 3. The kinetic friction F_K for small sliding velocities. Parameters are $\kappa = 1$, $N = 233$, $M = 144$, $b = 2/\pi \approx 0.637$. Using definition (7) the data has been obtained by numerical integration of (5). Each data point is the average over $500/v$ time units. In order to avoid averaging during transients the system has been evolved over 10^3 time units before starting averaging. The last state has been chosen as the initial value for the next data point with increased v. In order to get some information about the low-frequency fluctuations the averaging interval is chunked into ten pieces, each $50/v$ time units long, yielding ten values of F_K. The standard deviation of them are denoted by error bars.

FIG. 4. Main resonance, superharmonic and parametric resonance for $\kappa = 1$, $N = 233$, and $M = 144$. Resonance velocities of main resonance and superharmonic resonances in accordance with (30): $v_1^S \approx 0.337$, $v_2^S \approx 0.134$, $v_3^S \approx 0.071$, $v_4^S \approx 0.089$. Parametric resonance intervals in accordance with (34): First order: $[0.480, 0.614]$. Second order: $[0.197, 0.337]$. Part (a) shows a comparison between the approximation (31) (dotted line) and the numerically obtained solution of equation of the dynamical hull function (37) (solid line) for $\gamma = 0.5$ and $b = 1/\pi \approx 0.318$. Part (b) shows different solutions of (37) for $\gamma = 0.1$ and $2\pi b = 0.1$, 0.2, 0.5, 1 and 2. Solid (dotted) lines indicate stable (unstable) solutions. Part (c) compares the hull function solution (dashed line) with the full simulation of (5) (solid line and squares for increasing v, dotted line and triangles for decreasing v) for $\gamma = 0.1$ and $b = 1/(2\pi) \approx 0.159$. Details of the simulation are the same as in Fig. 3.

FIG. 5. Stroboscopic map of quasiperiodic and chaotic motion caused by first-order parametric resonance. The parameters are $\kappa = 1$, $N = 233$, $M = 144$, $\gamma = 0.1$, $v = 0.5$, and (a) $b = 1/(2\pi) \approx 0.159$, (b) $b = 3/(2\pi) \approx 0.478$. f_n is the lateral force $-\kappa/N \sum_j \xi_j$ at time $t = n/v$.

FIG. 6. The kinetic friction $F_K(v)$. Parameters are $\kappa = 1$, $N = 233$, $b = 3/(2\pi) \approx 0.478$, $\gamma = 0.1$, and (a) $c = 144/233$, (b) $c = 1$. Squares (triangles) connected by solid (dashed) lines denote the numerically obtained values for increasing (decreasing) sliding velocity v. The averaging procedure is the same as described in the caption of Fig. 3.

FIG. 7. Densities of the most important decay channels beyond the main resonance. The parameters are $\kappa = 1$ and (a) $c = (\sqrt{5} - 1)/2 \approx 0.618$, (b) $c = 1$.

FIG. 8. Coherent motion. The first five particles are shown. The parameters are $\kappa = 1$, $N = 233$, $M = 144$, $\gamma = 0.1$, $b = 3/(2\pi) \approx 0.478$, and $v = 1.06$.

FIG. 9. Dark envelope solitons embedded into the coherent motion seen in Fig. 8. The parameters are the same as in Fig. 8. The grey scale from dark to bright denotes the strength of the amplitude of the fast oscillations of the particles. The coherent motion is indicated by the regular stripes. There are three dark solitons traveling with three different velocities. At $j \approx 100$ and $t \approx 190$ two of them interact nondestructively.

Fig. 8 --- M. Weiss and F.J. Elmer

Fig. 7(a) --- M. Weiss and F.J. Elmer

(a)

density of decay channels

ρ_1^2

ρ_1^3

ρ_1^4

v
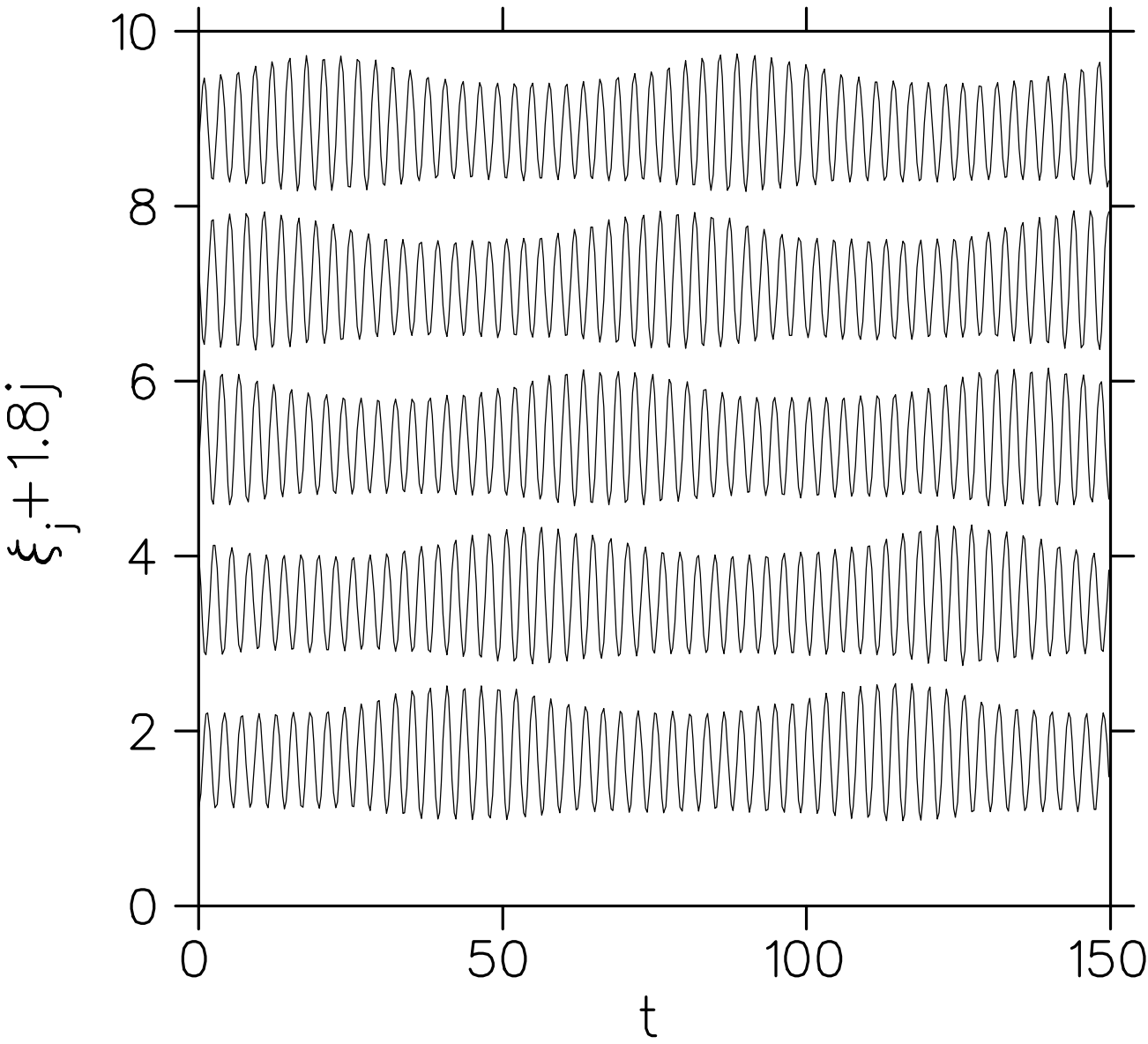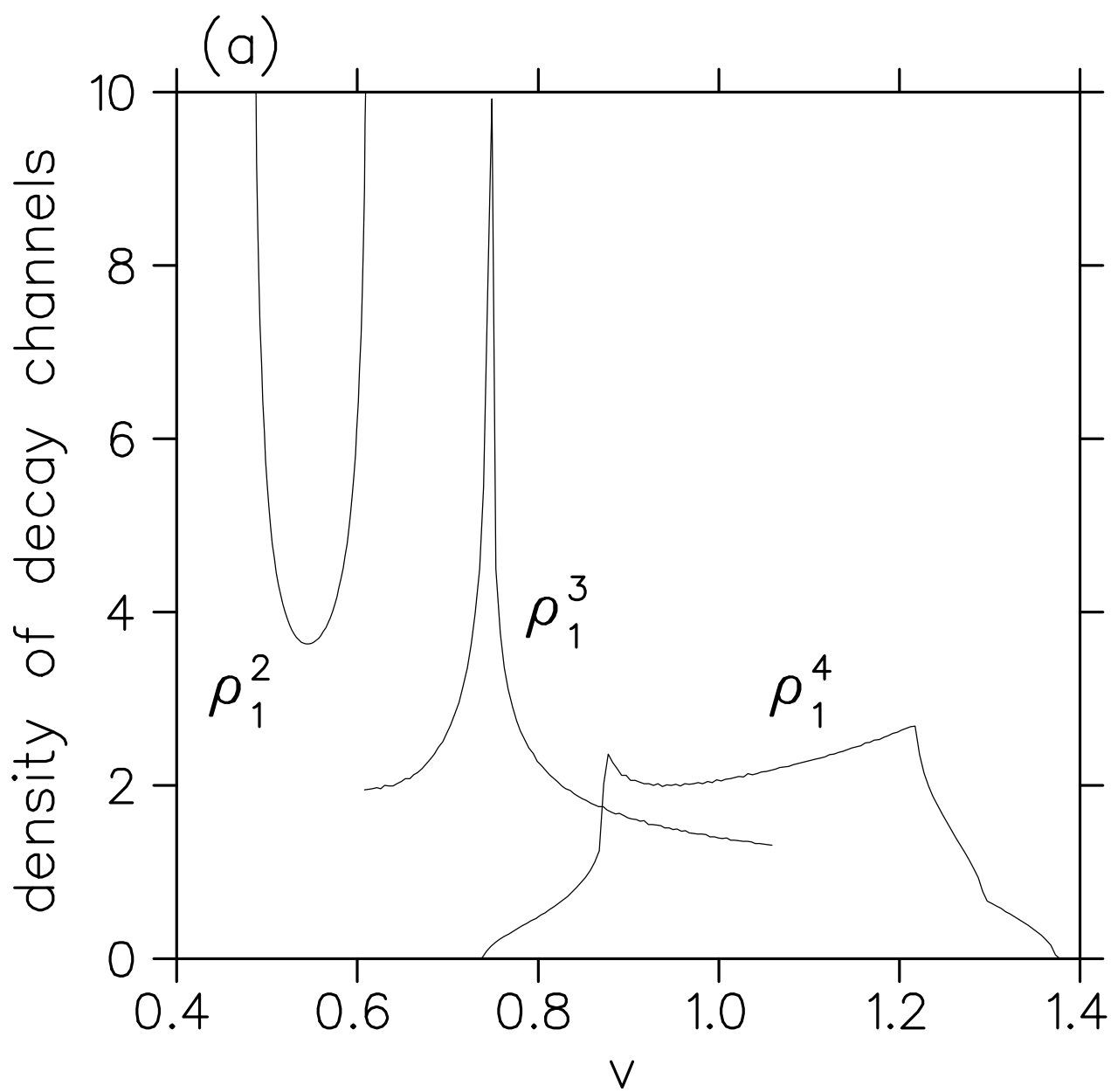
Fig. 7(b) --- M. Weiss and F.J. Elmer
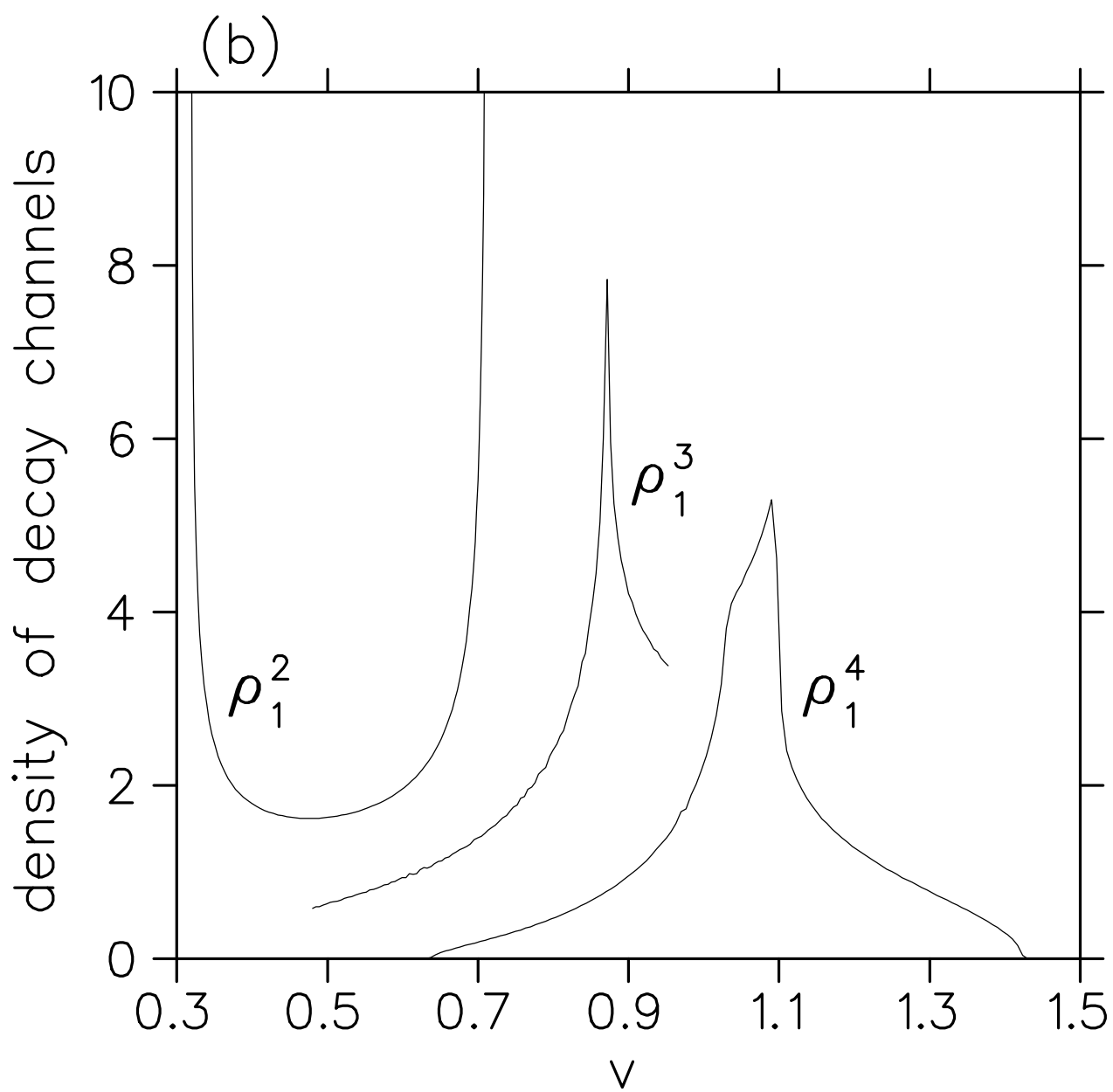
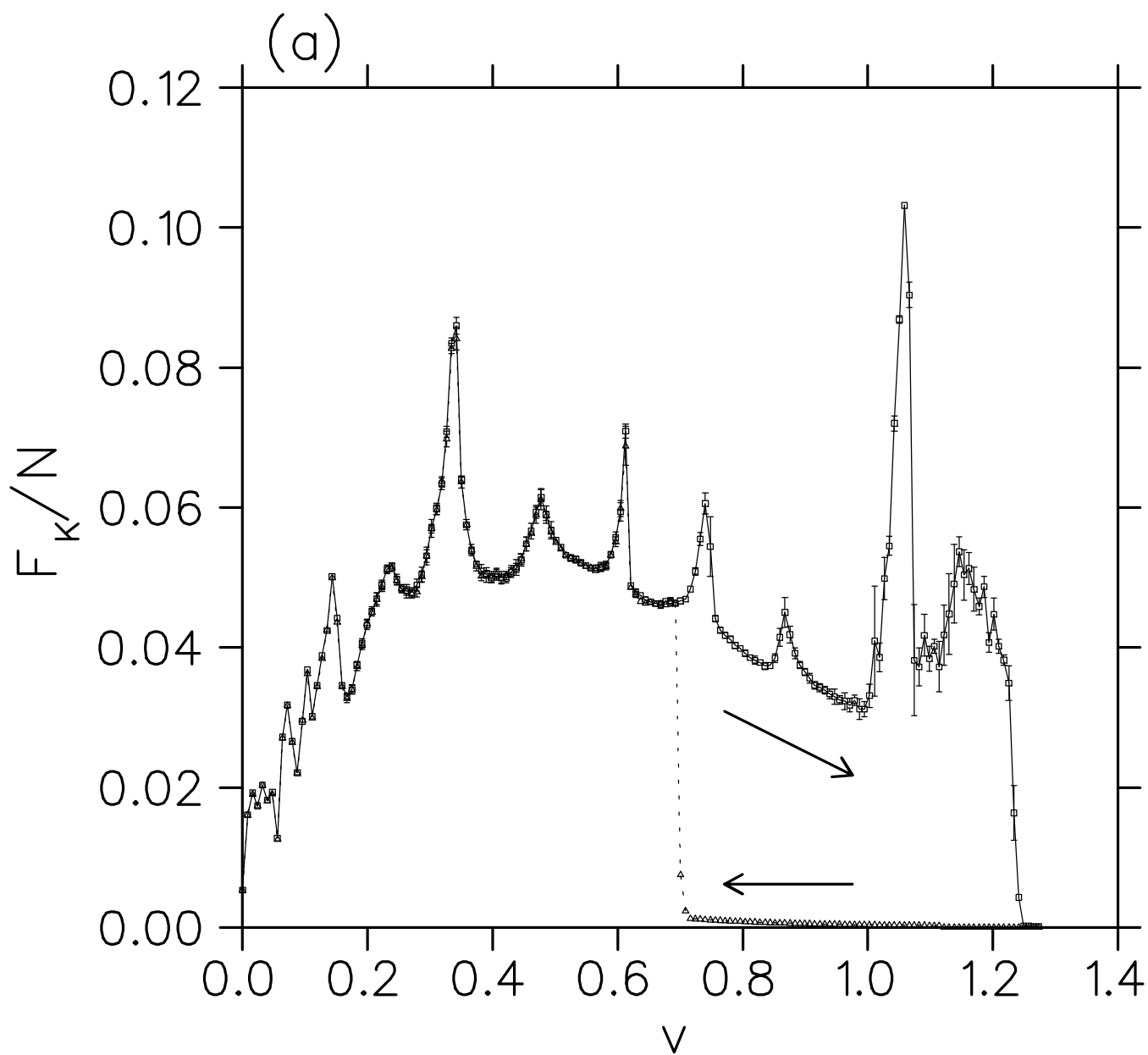Fig. 6(a) --- M. Weiss and F.J. Elmer
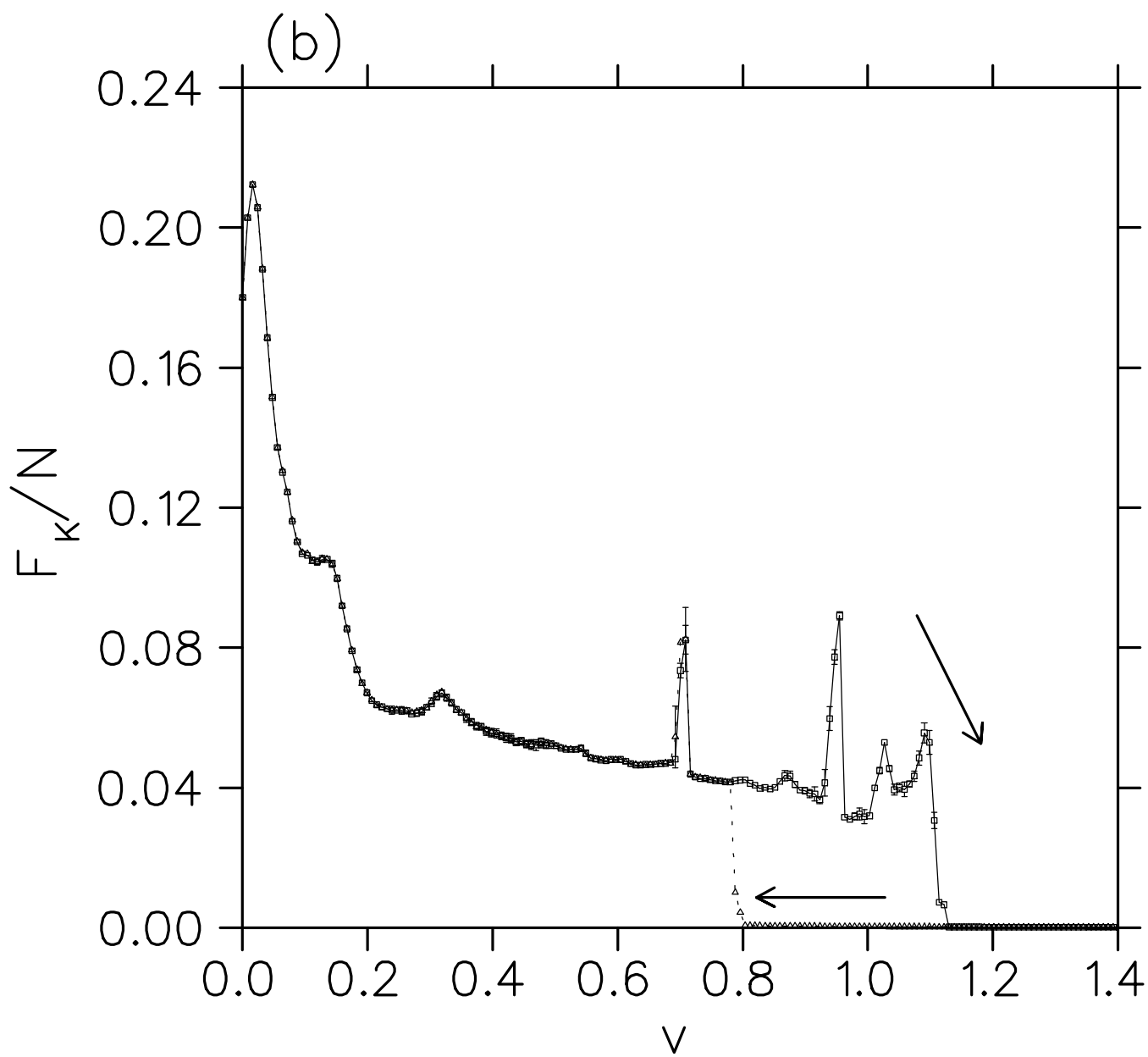
Fig. 6(b) --- M. Weiss and F.J. Elmer
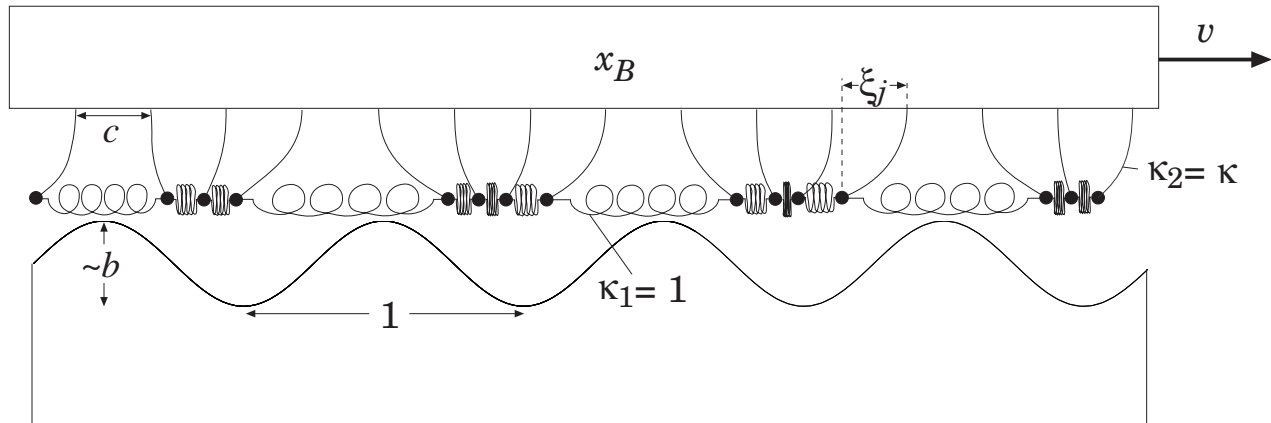

(b)

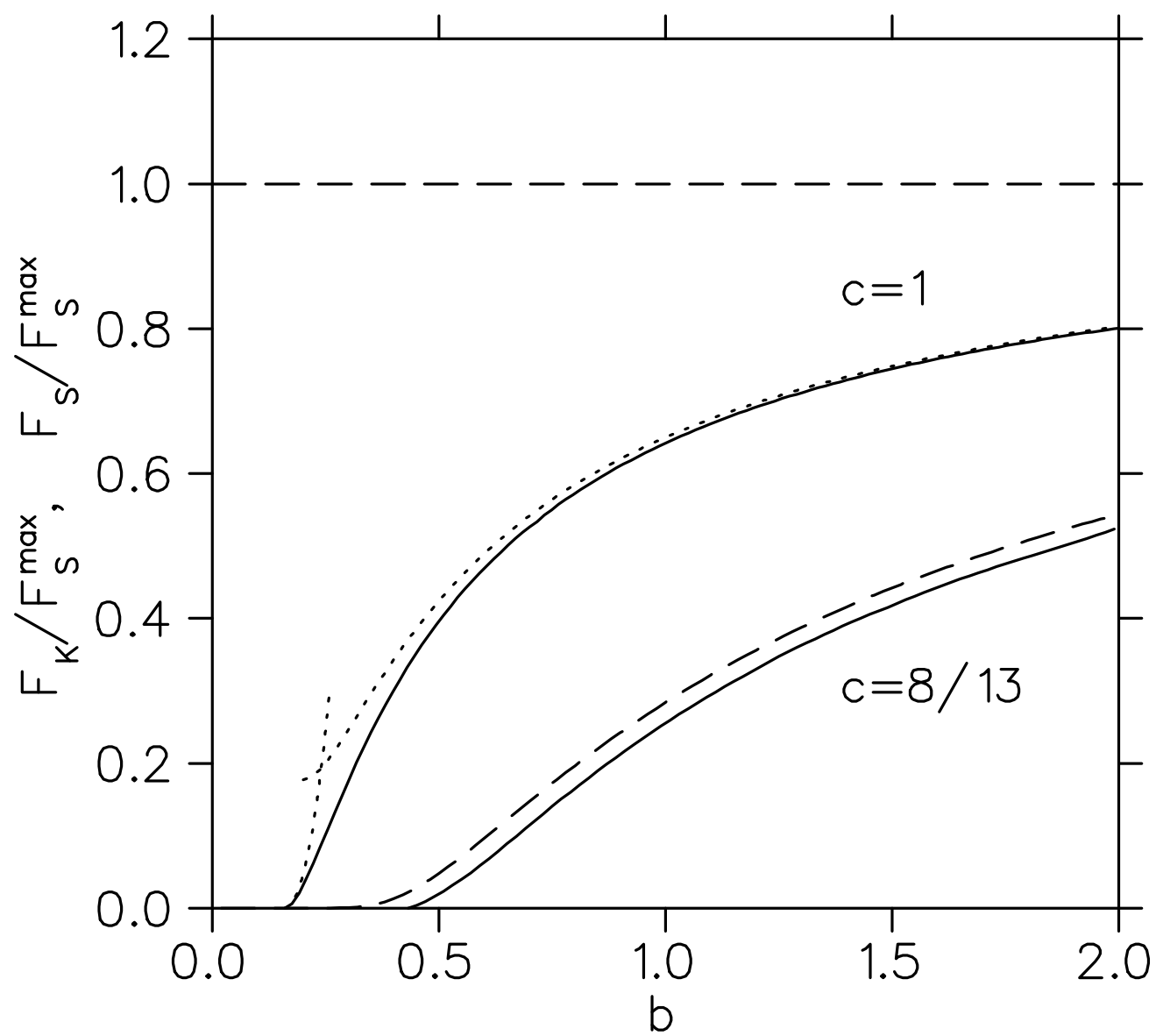Fig. 1 --- M. Weiss and F.J. Elmer

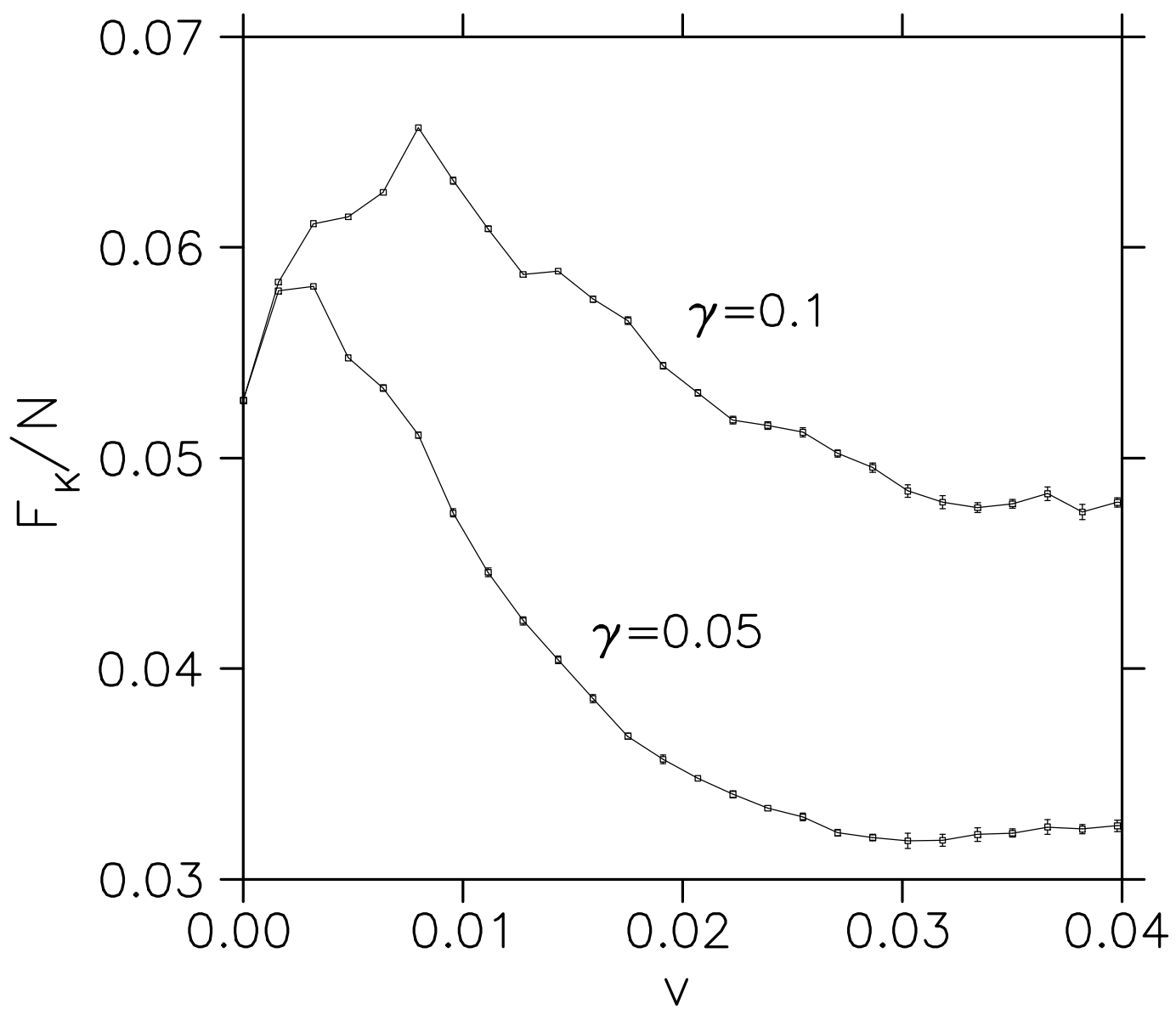Fig. 2 --- M. Weiss and F.J. Elmer

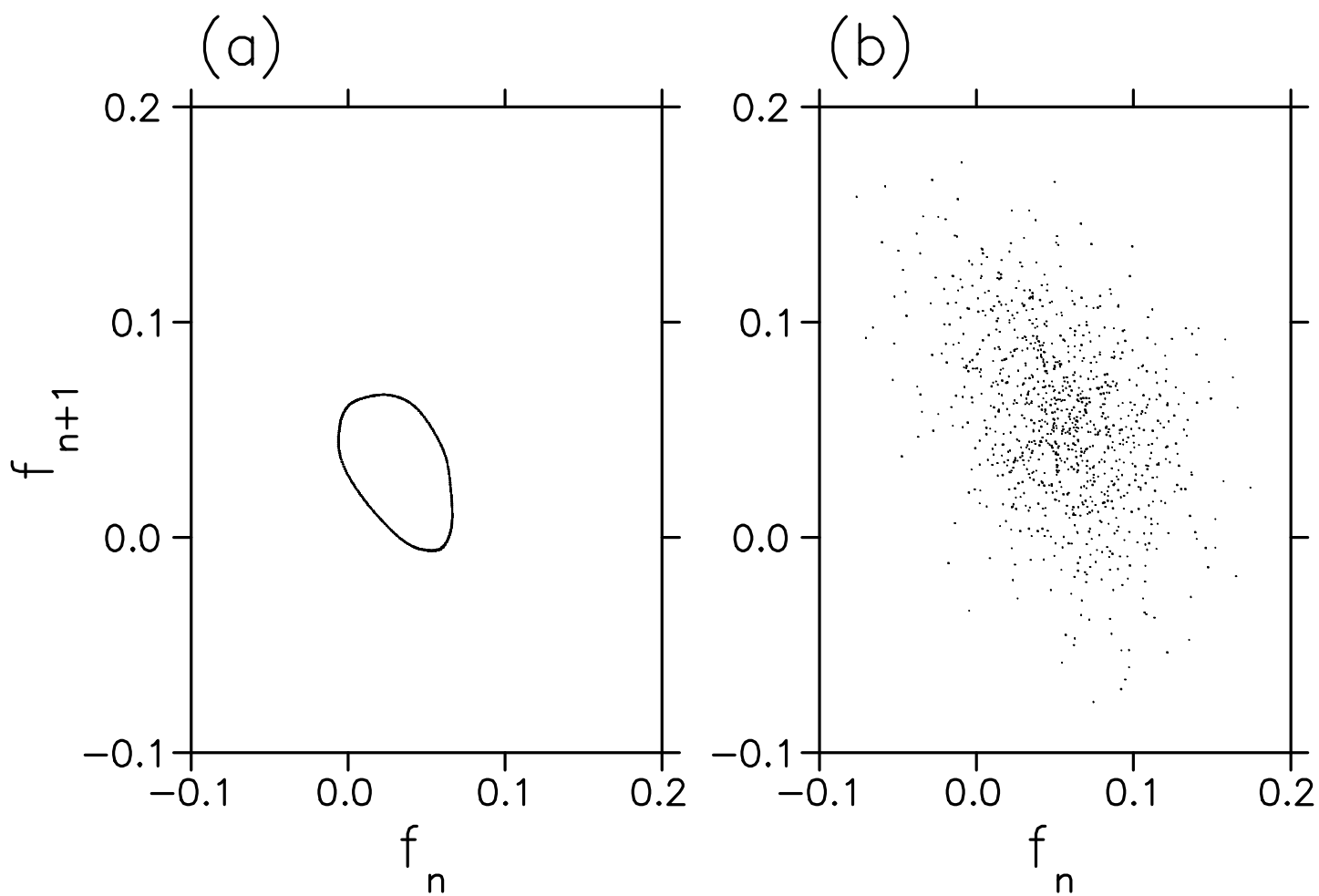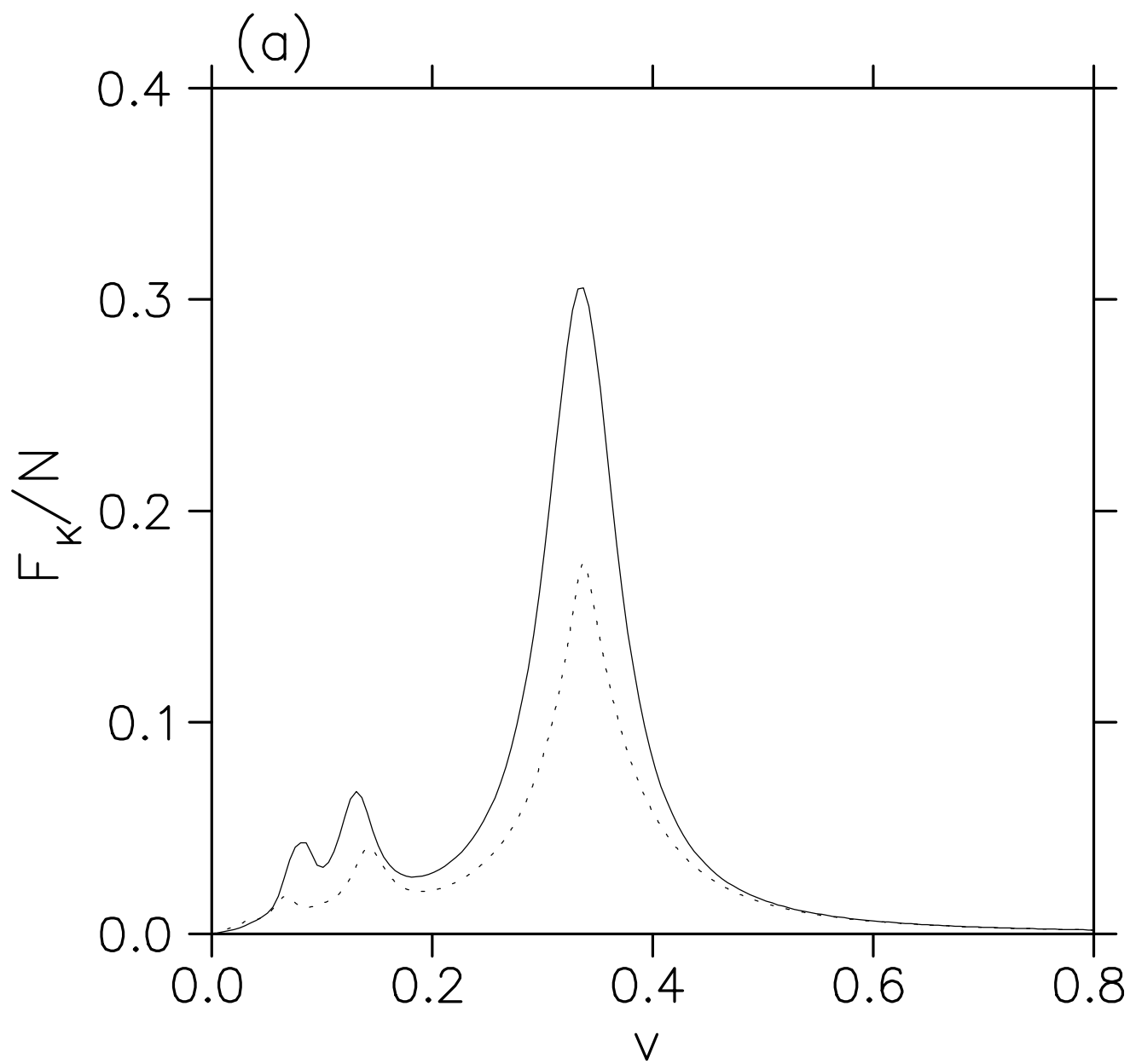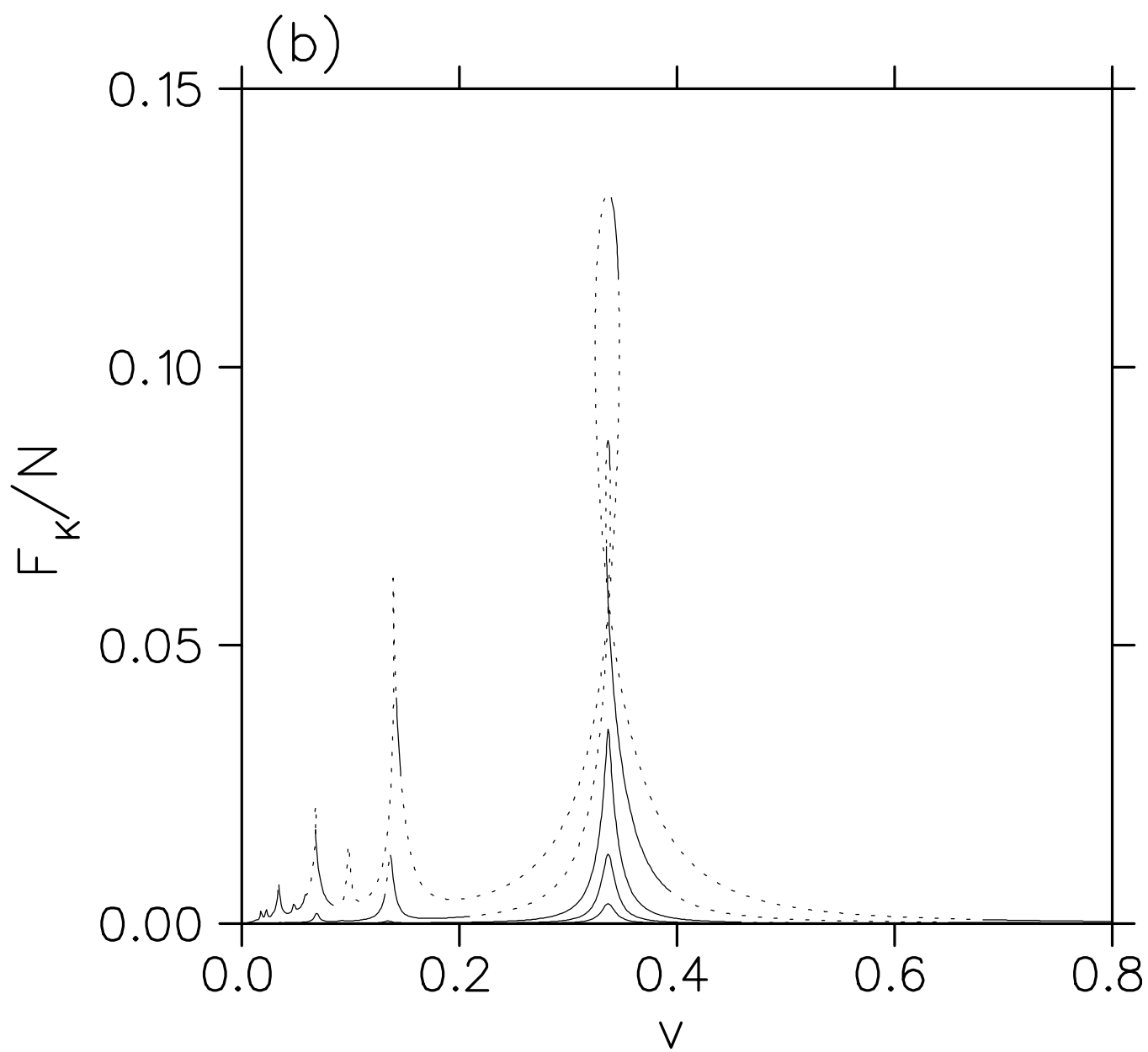Fig. 3 --- M. Weiss and F.J. Elmer

Fig. 5 --- M. Weiss and F.J. Elmer

Fig. 4(a) --- M. Weiss and F.J. Elmer
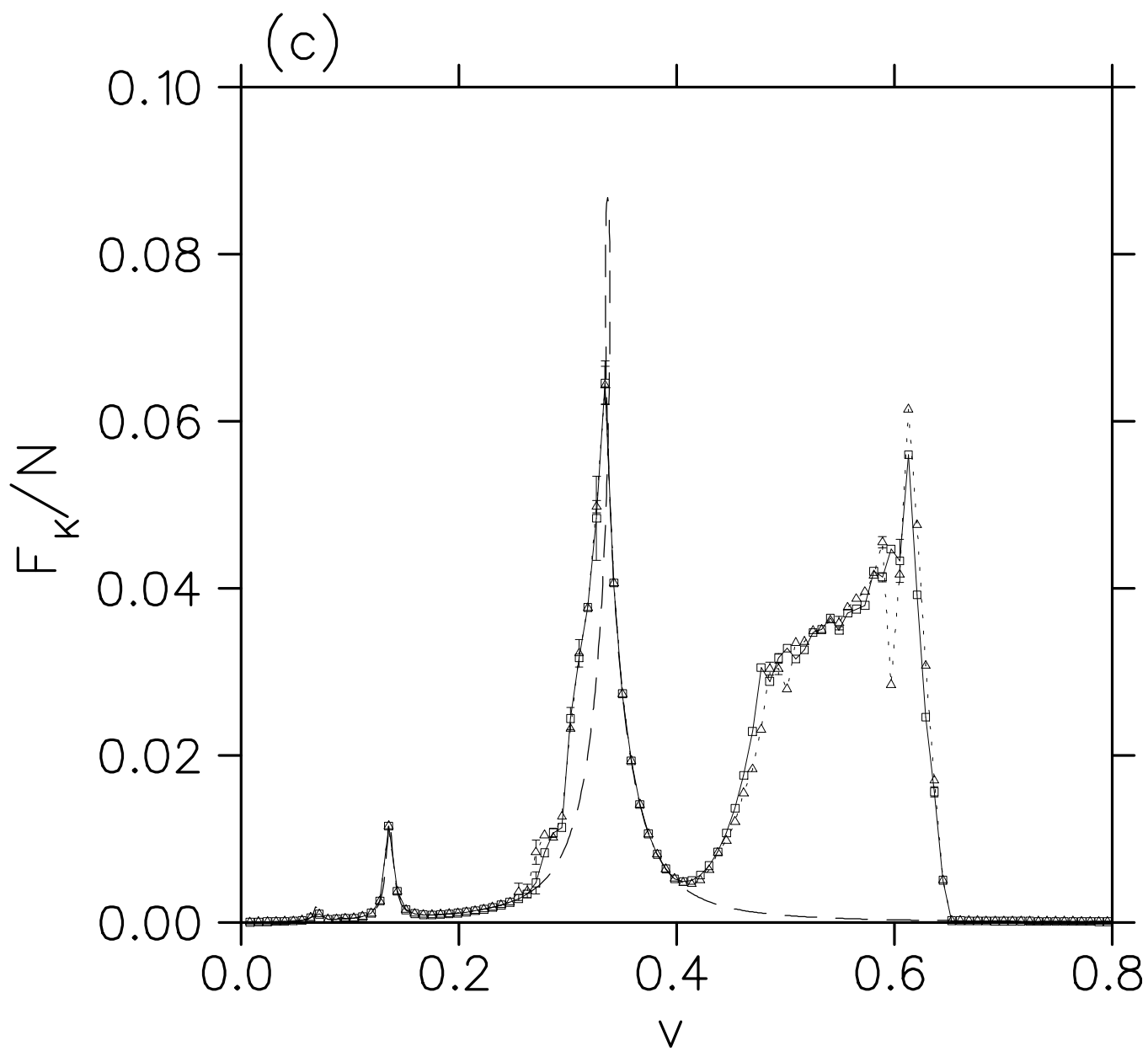
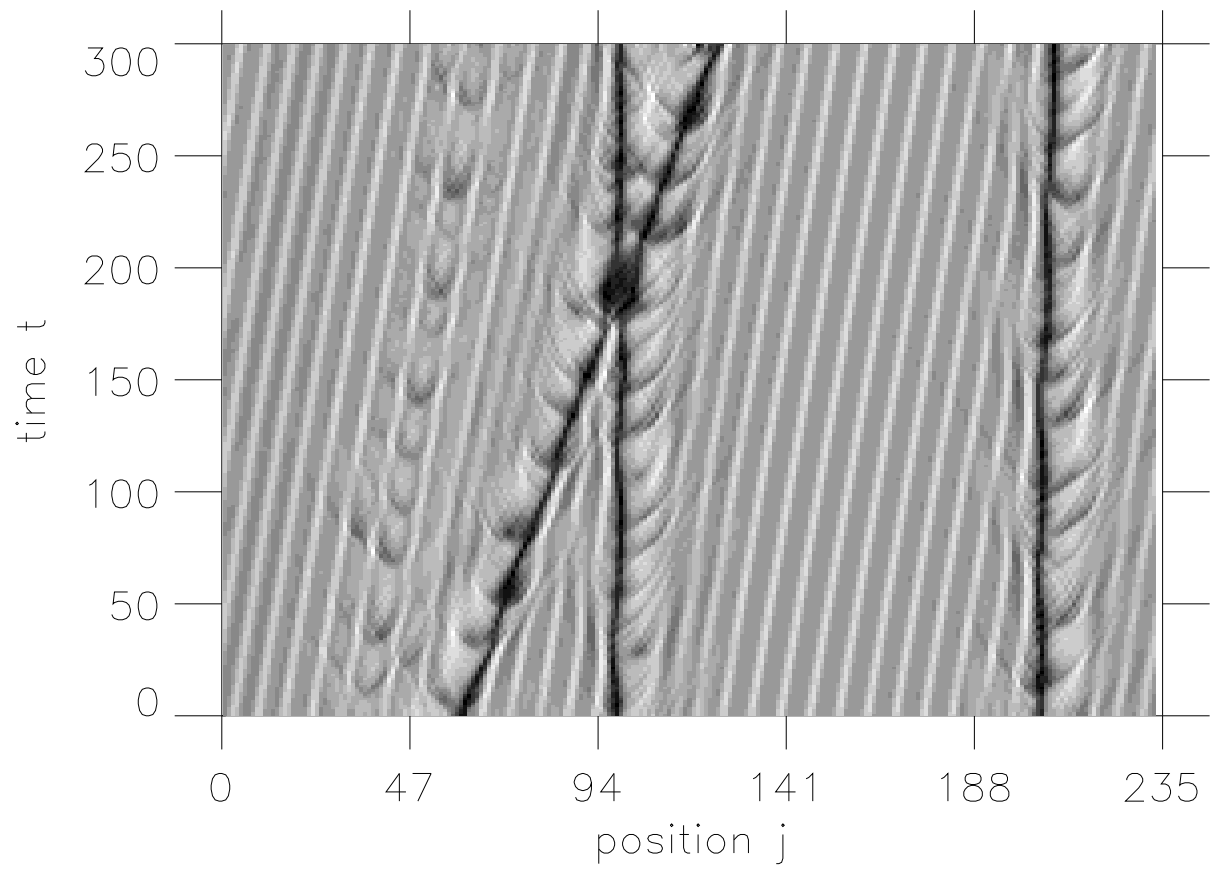Fig. 4(b) --- M. Weiss and F.J. Elmer

Fig. 4(c) --- M. Weiss and F.J. Elmer

Fig. 9 --- M. Weiss and F.J. Elmer